Divergence of *germ cell-less* roles in germ line development across insect species

Authors: Jonchee A. Kao[1], Ben Ewen-Campen[2,3], Cassandra G. Extavour[1,2,4]

[1]Department of Molecular and Cellular Biology, Harvard University, 16 Divinity Ave, Cambridge, MA 02138, USA

[2]Department of Organismic and Evolutionary Biology, Harvard University, 16 Divinity Ave, Cambridge, MA 02138, USA

[3]Current address: Department of Genetics, Blavatnik Institute, Harvard Medical School, Harvard University, Boston, MA 02115, USA

[4]Howard Hughes Medical Institute, Chevy Chase, MD, USA

Corresponding author: Cassandra G. Extavour

Email: extavour@oeb.harvard.edu

Phone: (617) 496-1935

ORCIDs: JAK 0000-0003-1701-3265; BE-C 0000-0002-4326-3033, CGE 0000-0003-2922-5855

Keywords: *Oncopeltus fasciatus*; *Gryllus bimaculatus*; germ cell specification; *torso*; pole cells

Abstract

During development, sexually reproducing animals must specify and maintain the germ line, the lineage of cells that gives rise to the next generation of animals. In the fruit fly *Drosophila melanogaster*, *germ cell-less* (*gcl*) is required for the formation of primordial germ cells in the form of cells that cellularize at the posterior pole of the embryo, called pole cells. Forming pole cells is a mechanism of germ cell formation unique to a subset of insects. Even though most animals do not form pole cells as primordial germ cells, *gcl* is conserved across Metazoa, raising the question of how this conserved gene acquired its central role in the evolutionarily derived process of pole cell formation. Here, we examine the functions of *gcl* in two other insects with different modes of germ cell specification: the milkweed bug *Oncopeltus fasciatus* and the cricket *Gryllus bimaculatus*. We found that *gcl* is involved in germ cell development, but not strictly required for germ cell specification, in *O. fasciatus*, although it appears to function through a mechanism different from that in *D. melanogaster*. In contrast, we could not detect any impact on the embryonic germ line upon *gcl* knockdown in *G. bimaculatus*. This work serves as a case study into how the roles of genes in the process of germ line development can change over evolutionary time across animals.

Keywords: Germ cells, pole cells, *Oncopeltus fasciatus*, *Gryllus bimaculatus*, Hemimetabola, milkweed bug, cricket, Torso

Highlights

- *germ cell-less* knockout reduces germ cell number in *Oncopeltus fasciatus*.
- *germ cell-less* knockdown does not affect germ cell number in *Gryllus bimaculatus*.
- The genetic mechanisms through which *gcl* affects germ cell number have diverged among insects.

Graphical abstract

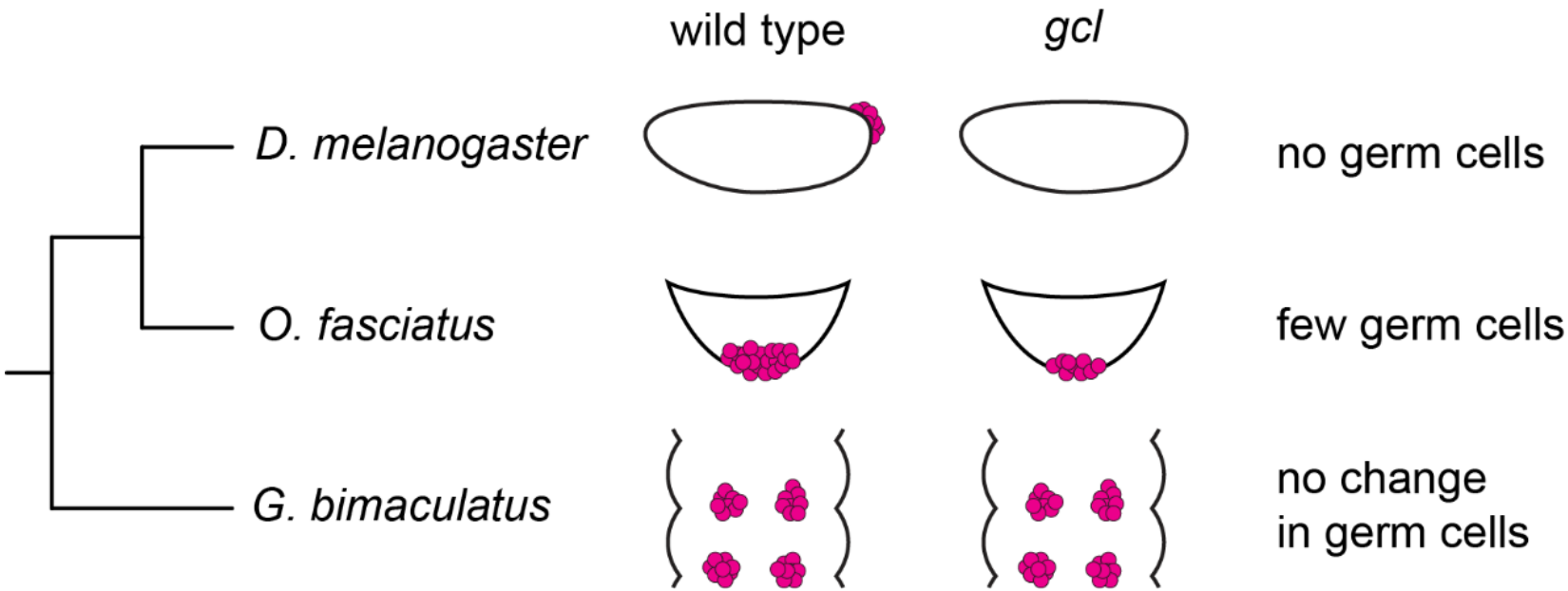

48 **Introduction**

49 One of the most crucial processes in animal development is the specification and
50 maintenance of the germ line, the lineage of cells uniquely capable of giving rise to the next
51 generation of animals (Extavour and Akam, 2003). Despite the importance of this process,
52 mechanisms of germ line development vary widely even within closely related taxa, including
53 across insects (Extavour and Akam, 2003). For example, in the fruit fly *Drosophila*
54 *melanogaster*, germ cells first appear at the posterior pole of the embryo very early in
55 embryogenesis, before cellularization occurs in the rest of the embryo (Huettner, 1923). The
56 formation of germ cells in embryos of this fly depends on the presence of the germ plasm, a
57 specialized region of the cytoplasm at the posterior pole containing maternally synthesized
58 RNAs and proteins that collectively direct the formation and specification of germ cells
59 (Illmensee and Mahowald, 1974). In contrast, germ cells in the cricket *Gryllus bimaculatus* are
60 first detectable comparatively later in embryogenesis, after segmentation of the abdomen has
61 begun (Ewen-Campen et al., 2013a). There is no evidence of germ plasm in cricket embryos, and
62 germ cells are thought to be specified instead by inductive signals from neighboring cells,
63 including BMP signaling (Donoughe et al., 2014; Ewen-Campen et al., 2013a). In yet another
64 mechanism of insect germ cell specification, germ cells of the milkweed bug *Oncopeltus*
65 *fasciatus* appear at a stage intermediate between those of *D. melanogaster* and *G. bimaculatus*,
66 after blastoderm cellularization but before abdominal segmentation (Butt, 1949; Ewen-Campen
67 et al., 2013b). There is also no evidence of germ plasm in embryos of this bug (Ewen-Campen et
68 al., 2013b), but specific germ cell specification signals have not been identified.

69 Despite the variation in modes of germ line development across species, many genes
70 involved in this process are conserved. These include *vasa* and *piwi*, which are commonly used

71 as germ cell markers in many different animals (Ewen-Campen et al., 2010). *germ cell-less* (*gcl*)
72 is also sometimes used as a germ cell marker, but its role in germ line development is less well
73 understood (Jongens et al., 1992). Embryos laid by *D. melanogaster* females homozygous for a
74 loss of function mutation in *gcl* have significantly fewer germ cells than controls, if any (Jongens
75 et al., 1994, 1992). The gene is thought to have a role in suppressing somatic cell fate by
76 targeting the receptor tyrosine kinase Torso for degradation (Colonnetta et al., 2021; Pae et al.,
77 2017). *gcl* is also required for germ cell transcriptional quiescence in flies (Leatherman et al.,
78 2002). However, *gcl* is not required for germ cell specification in the mouse *Mus musculus* nor in
79 the flour beetle *Tribolium castaneum*, but it is required for proper mouse spermatogenesis
80 (Ansari et al., 2018; Kimura et al., 2003). Outside the germ line, *gcl* plays a role in establishing
81 the anterior–posterior axis in *T. castaneum* (Ansari et al., 2018). Despite the wide divergence in
82 their physiological roles, *gcl* homologs are highly conserved in amino acid sequence, with 45%
83 similarity between homologs from *D. melanogaster* and *M. musculus*. In addition, these
84 homologs appear to share at least some biochemical functions, since the mouse *gcl* homolog can
85 partially restore germ cell formation in a *gcl*-null *D. melanogaster* embryo, though not to wild
86 type numbers (Leatherman et al., 2000). *gcl* expression has also been observed in the embryonic
87 germ line in other arthropod species (Ewen-Campen et al., 2013a; Gupta and Extavour, 2013).
88 However, to our knowledge, functional tests of whether *gcl* is required for insect germ line
89 development or function remain limited to *D. melanogaster* and *T. castaneum*.

90 Here, we examine the function of *germ cell-less* in the embryonic and adult germ lines of
91 *O. fasciatus* and *G. bimaculatus*. Our data suggest that *gcl* is not required for germ cell
92 specification nor for adult gametogenesis in either species. However, *gcl* mutant *O. fasciatus*
93 embryos have significantly fewer germ cells than wild type. Knockdown of *Of-torso* does not

affect germ cell number, suggesting that *gcl* in this species affects germ cell number through a different mechanism from that in *D. melanogaster*. Overall, these studies into *gcl* function across species inform our understanding of the evolution of gene function in germ line development.

Materials and Methods

Gene identification

germ cell-less. *Of-germ cell-less* is annotated as OFAS015300 on Scaffold 2113 of the current *O. fasciatus* genome assembly (Panfilio et al., 2019). *Gb-germ cell-less* is annotated as GBIM03474 on Scaffold 14 of the current *G. bimaculatus* genome assembly (Ylla et al., 2021). We amplified both genes from mixed stage embryonic cDNA of the respective species to verify the full-length coding sequences.

Of-torso. A tBLASTn search was performed on the *O. fasciatus* genome (Panfilio et al., 2019) using *D. melanogaster* Torso as a query, and a reciprocal BLASTp was performed on the top results with e-value < 1e–40. Of the initial results, OFAS005359 on Scaffold 336 returned *torso* orthologs from other insects. A reciprocal BLASTp search using the adjacent upstream annotated gene, OFAS005360, also returned *torso* orthologs from other insects. PCR was performed from mixed stage embryonic cDNA to confirm that OFAS005359 and OFAS005360 correspond to the same transcript. To obtain full-length sequence, RACE was performed using the SMARTer RACE 5’/3’ Kit (Takara Bio 634859) following manufacturer’s instructions.

114 The initial tBLASTn search using *D. melanogaster* Torso as a query also returned
115 OFAS025175 as a result. A reciprocal BLASTp search using the predicted peptide sequence of
116 this hit returned *fgf receptor* orthologs from other insects. Since the FGF receptor is a family of
117 receptor tyrosine kinases closely related to Torso (Duncan et al., 2013), we wanted to include
118 OFAS025175 for phylogenetic analysis. Therefore, we performed RACE using the SMARTer
119 RACE 5'/3' Kit to obtain the full-length sequence of this gene. Full length sequences for both
120 *Of-torso* and *Of-fgfr* have been deposited at GenBank with accession numbers PV361543 and
121 PV361544, respectively.

122 Phylogenetic analysis was performed using MEGA 11 (Tamura et al., 2021). Insect
123 orthologs of Torso were aligned using MUSCLE (Edgar, 2004) along with orthologs of Ret
124 oncogene and FGF receptor, which are the closest related families of receptor tyrosine kinases
125 (Duncan et al., 2013). The multiple sequence alignment was used to generate a gene tree using
126 the Maximum Likelihood method with the JTT substitution model (Jones et al., 1992), a discrete
127 Gamma-distributed rate model and 1000 bootstrap replicates.

128

129 *Molecular biology*

130 *RNA extraction and cDNA synthesis*. Embryos or tissues of interest were homogenized in TRIzol
131 (Invitrogen 15596026), and RNA was extracted with phenol–chloroform extraction and
132 isopropanol precipitation. cDNA was synthesized with SuperScript III First-Strand Synthesis
133 SuperMix for qRT-PCR (Invitrogen 11752250) following manufacturer's instructions.

134 *Cloning and* in vitro *transcription.* Fragments of genes of interest were PCR-amplified from
135 embryonic cDNA and each cloned into the pGEM-T Easy vector (Promega A137A) using

136 manufacturer's instructions. A fragment of *gfp* was subcloned from an existing plasmid
137 containing the *gfp* sequence. Insertion was confirmed by Sanger sequencing. Primers used are
138 listed in Supplemental Table 1.

139 For *in situ* probe synthesis, gene fragments were PCR-amplified from plasmids using T7
140 and Sp6 primers. *In vitro* transcription was performed using T7 RNA polymerase (Promega
141 P2075) or Sp6 RNA polymerase (Roche 10810274001) with DIG RNA labeling mix (Roche
142 11277073910). 100 ng of template was used for a 20-µl reaction run at 37°C overnight. RNA
143 was purified with LiCl/ethanol precipitation, then resuspended in 20 µl DEPC-treated water.
144 Concentration was measured using a NanoDrop Spectrophotometer (ThermoFisher), and the
145 sample was diluted to 100 ng/µl with hybridization buffer (50% formamide, 1x phosphate-
146 buffered saline (PBS), 5x saline–sodium citrate (SSC), 0.1% Triton X-100, 0.1% CHAPS, 5 mM
147 EDTA, 50 µg/mL heparin, 1 µg/mL yeast tRNA). Probes were stored at −20°C.

148 For double-stranded RNA (dsRNA) synthesis, gene fragments were PCR-amplified from
149 plasmids using a forward T7 primer and a reverse primer containing both T7 and Sp6 promoter
150 sequences to generate a template for *in vitro* transcription with the T7 promoter sequence on both
151 ends. *In vitro* transcription was performed using the MEGAscript T7 Transcription Kit
152 (Invitrogen AM13345). 100 ng of template was used for an 80-µl reaction run at 37°C overnight.
153 RNA was purified with LiCl/ethanol precipitation, then resuspended in 100 µl DEPC-treated
154 water. To anneal the two strands, this solution was heated to 95°C on a heat block for 5 minutes,
155 then allowed to cool slowly by leaving the tube on the heat block with the power switched off. A
156 1:10 dilution of annealed RNA was analyzed using a NanoDrop Spectrophotometer
157 (ThermoFisher) to measure its concentration and purity, then run on a 1% agarose gel to confirm
158 its size and integrity. For embryonic RNAi, dsRNA was diluted in DEPC-treated water to 2 µg/µl

159 (*O. fasciatus*) or 5 µg/µl (*G. bimaculatus*), with 0.05% phenol red. For *G. bimaculatus* adult
160 RNAi, dsRNA was diluted to 7.5 µg/µl in DEPC-treated water.

161 *CRISPR/Cas9-mediated mutagenesis*. Alt-R S.p. Cas9 Nuclease V3 (cat. #1081059) and Alt-R
162 CRISPR-Cas9 tracrRNA (cat. #1072533) were ordered from IDT, along with gene-specific Alt-R
163 CRISPR-Cas9 crRNA. tracrRNA and crRNA were resuspended to 100 µM in Nuclease-Free
164 Duplex Buffer (IDT cat. #11-01-03-01). 5 µl of each RNA were combined in a PCR tube, heated
165 to 95°C for 5 minutes, and allowed to cool to room temperature to form 50 µM gRNA duplex. 3
166 µl gRNA and 2 µl Cas9 protein (10 µg/µl or ~62 µM) were combined in a PCR tube and
167 incubated at room temperature for 10 minutes to form Cas9/gRNA ribonucleoprotein complex
168 (RNP) at roughly 25 µM. Finally, RNP was diluted tenfold in 1x PBS with 0.05% phenol red.

169

170 *Of-Vasa antibody generation*

171 A rabbit polyclonal antibody was raised against a recombinant *Of*-Vasa protein fragment
172 (McGill Biology CIAN facility, Canada). The sequence encoding the 565 C-terminal amino acids
173 of *Of*-Vasa, the stop codon and the first 96 base pairs of 3' UTR (GenBank accession KC261571
174 (Ewen-Campen et al., 2013b)) was cloned into the pET151/dTOPO expression vector (Invitrogen
175 K151-01), thus introducing an N-terminal 6x-polyhistidine tag. Protein expression was induced
176 in *E. coli* BL21 (DE3) by addition of IPTG to a final concentration of 0.25 mM and shaking at
177 30°C for four hours. The overexpressed proteins were highly insoluble, so the cell pellets were
178 disrupted by sonication in non-denaturing buffer, and the soluble fraction was separated by
179 centrifugation and discarded. The pellet was resuspended in 8 M urea (crude prep). Crude preps
180 were further purified by SDS gel-purification. Protein bands were excised from the gel after

181 reverse staining with zinc chloride and the proteins were collected by electroelution. Acetone
182 precipitation was performed, and the precipitated protein was washed and resuspended in 8 M
183 urea. Protein concentration was adjusted to 1–2 mg/mL for injection. Rabbits were injected using
184 a standard 80-day protocol with three boosts after the initial injection; the final bleed was
185 performed after 87 days. The serum was processed by addition of sodium azide to 0.02% (w/v).
186 The antibody was affinity-purified against bacterially expressed *Of*-Vasa protein.

187

188 *Embryo microinjection*

189 Needles for injection were made by pulling glass capillaries (World Precision Instruments
190 1B100-4) with a Sutter P-97 Flaming/Brown micropipette puller. Needle tips were manually
191 opened with fine forceps just prior to injection. Eggs were injected with a Narishige IM300
192 microinjector.

193 *O. fasciatus* were allowed to lay eggs in dry cotton for four hours, after which eggs were
194 picked out of the cotton for injection. Two glass microscope slides were taped together with
195 double-sided tape to create a ledge with exposed double-sided tape against which embryos were
196 lined up. Eggs were then submerged in tap water for at least 20 minutes to soften the eggshell
197 before injection. Slides with injected eggs were kept at 28°C to continue development until the
198 desired age.

199 *G. bimaculatus* were allowed to lay eggs in wet cotton for four hours, after which eggs
200 were washed out of the cotton for injection. Eggs were aligned in grooves (570 µm wide × 2930
201 µm long × 650 µm deep) made in 2% agarose in Milli-Q water using a custom mold as
202 previously described (Donoughe et al., 2018). Eggs were injected while submerged in 1x PBS.

203 After injection, the solution was replaced with fresh 1x PBS. Injected eggs were kept submerged
204 in 1x PBS at 28°C overnight. The following day, dead embryos, if any, were removed, and the
205 remaining eggs were transferred onto damp Kimwipes in a covered Petri dish kept at 28°C to
206 continue development. Three days after injection, eggs were submerged in tap water again and
207 monitored every day until they reached the desired stage for dissection.

208

209 *Embryo dissection and fixation*

210 *O. fasciatus* eggs were stuck to the bottom of a 60-mm Petri dish with double-sided tape
211 and a slit was created in the eggshell with a microscalpel. 1x PBS with 4% paraformaldehyde
212 (PFA) was then poured into the dish to fix the embryos for 30 minutes at room temperature,
213 followed by at least three washes with PBT (1x PBS with 0.1% Triton X-100). Embryos were
214 then dissected free of their yolk in PBT with fine forceps. Embryos were washed at least three
215 times with PBT at room temperature before continuing with staining or dehydration in methanol.

216 *G. bimaculatus* embryos were dissected free of their yolk in 1x PBS with fine forceps and
217 fixed overnight in 1x PBS with 4% PFA at 4°C. The following morning, they were washed at
218 least three times with PBT at room temperature before continuing with staining or dehydration in
219 methanol.

220

221 *G. bimaculatus adult RNA interference (RNAi)*

222 2 µl dsRNA was injected into the abdomen of an adult cricket with a Hamilton syringe
223 through the base of a metathoracic leg. Gonads were dissected seven days after injection for
224 analysis.

225

226 *Colorimetric in situ hybridization*

227 Dissected embryos were stored in methanol at −20°C overnight or longer before *in situ*
228 hybridization. After rehydration in PBT and washing in hybridization buffer, embryos were
229 hybridized overnight in a 70°C water bath with 1 ng/µl probe in hybridization buffer. The
230 following day, the following series of 20-minute washes were performed at 70°C: once in
231 hybridization buffer, three times in wash 1 (2x SSC, 0.1% CHAPS) and three times in wash 2
232 (0.2x SSC, 0.1% CHAPS). Embryos were then washed three times for ten minutes each at room
233 temperature in KTBT (1x Tris-buffered saline with KCl and 0.1% Triton X-100) followed by an
234 hour-long incubation at room temperature in *in situ* blocking solution (1x PBS, 0.1% Tween-20,
235 5% NGS, 2 mg/mL bovine serum albumin, 1% dimethyl sulfoxide). Embryos were incubated for
236 two hours at room temperature with sheep anti-digoxigenin–AP (Roche 11093274910), diluted
237 1:2000 in *in situ* blocking solution, then washed at least four times over two hours with KTBT
238 and incubated in KTBT overnight at 4°C. The following day, embryos were washed with NTMT
239 (100 mM Tris pH 9.5, 100 mM NaCl, 50 mM $MgCl_2$, 0.1% Tween-20), then developed in the
240 dark at 37°C with NBT/BCIP in NTMT with 5% polyvinyl alcohol. Development was monitored
241 at least every hour under a dissection microscope. To stop development of the enzymatic
242 reaction, embryos were washed in PBT, incubated with 5 ng/µl Hoechst 33342 in PBT at room
243 temperature for an hour, post-fixed in 4% PFA in PBS, then incubated in 70% glycerol before
244 mounting in 100% glycerol.

245

246 *Immunohistochemistry*

247 Embryos were incubated in blocking solution (PBT with 5% normal goat serum (Jackson
248 ImmunoResearch 005-000-121)) for one hour at room temperature, then incubated overnight at
249 4°C with primary antibodies diluted in blocking solution. The following day, embryos were
250 washed for at least four times over four hours with PBT, incubated for an hour in blocking
251 solution, then incubated overnight at 4°C with secondary antibodies diluted in blocking solution.
252 Finally, embryos were washed in PBT, post-fixed in 4% PFA in PBS, then incubated in 70%
253 glycerol before mounting in glycerol. Antibody staining was also performed with a no-primary
254 control.

255 Primary antibodies used were: rabbit anti-*Gb*-Piwi (Ewen-Campen et al., 2013a) at a final
256 concentration of 1:300; rabbit anti-*Of*-Vasa at 1:100; mouse anti-α-tubulin (DM1A; Sigma
257 T9026) at 1:100; rabbit anti-β-catenin (Sigma C2206) at 1:500; and mouse anti-RNA polymerase
258 II (H5; Covance MMS-129R) (Bregman et al., 1995; Warren et al., 1992) at 1:100. Secondary
259 antibodies used were goat anti-rabbit conjugated to Alexa Fluor 647 (Invitrogen A-21246), goat
260 anti-rabbit Alexa Fluor 488 (Invitrogen A-11008), goat anti-rabbit Alexa Fluor 568 (Invitrogen
261 A-11011), donkey anti-mouse Alexa Fluor 488 (Invitrogen A-21202), and goat anti-mouse Alexa
262 Fluor 647 (Invitrogen A-21236). All secondary antibodies were used at a final concentration of
263 1:400 along with Hoechst 33342 (Sigma B2261) at 5 ng/µl.

264 Embryos were imaged on a Nikon CSU-W1 spinning disk inverted confocal microscope
265 with 10x air or 20x air objectives or a Zeiss AxioObserver inverted compound microscope with
266 10x air or 20x air objectives. Images were analyzed in Fiji.

267

268 *Quantitative RT-PCR*

269 Quantitative RT-PCR was performed on an AriaMx Real-time PCR system (Agilent)
270 using PerfeCTa SYBR Green SuperMix, Low ROX (Quantabio 95056). Fold-change differences
271 were calculated using the $\Delta\Delta C_t$ method for RNAi experiments. Expression levels were
272 normalized against *Of-gapdh* or *Gb-β-tubulin*. All primers used are listed in Supplemental Table
273 1.

274 **Results**.

275 *germ cell-less expression across insect species.*

276 During oogenesis in *D. melanogaster*, Gcl protein is detectable at the nuclear membrane
277 of nurse cells and oocytes (Moore et al., 2009). In addition, *gcl* transcripts are transcribed by
278 nurse cells, transported into the oocyte and deposited at the oocyte posterior, where they remain
279 as part of the germ plasm into early embryogenesis (Jongens et al., 1992). These transcripts are
280 translated into protein starting at the cleavage stages of embryogenesis (Jongens et al., 1992).
281 Gcl protein is localized to the nuclear membranes of germ cells after they form and remains
282 detectable in germ cells until mid-gastrulation, when germ cells enter the primordial midgut
283 (Jongens et al., 1992). We asked whether *gcl* is also expressed in other insect embryos at the time
284 and place of germ cell specification.

285 We assessed *gcl* transcript levels using quantitative RT-PCR on *O. fasciatus* embryos
286 collected in 12-hour windows spanning the first four days of embryogenesis. *Of-gcl* transcripts
287 were detected at the highest levels 24–36 hours after egg-lay at 28°C (Figure 1A). This window
288 corresponds to the late blastoderm stage, when germ cells are first distinguishable (Ewen-

289 Campen et al., 2013b), and the beginning of germ band elongation. We speculate that this peak in
290 expression is likely due to zygotic rather than maternal expression, since it is higher than
291 expression in freshly laid eggs. However, we were unable to detect *Of-gcl* transcripts by *in situ*
292 hybridization above background levels in embryos at any stage of development, nor in adult
293 ovaries or testes (Supplemental Figure 1A–B).

294 We similarly assessed *gcl* transcript levels using qRT-PCR on *G. bimaculatus* embryos
295 collected in 8-hour windows spanning the first two days of embryogenesis and 24-hour windows
296 spanning the following eight days of embryogenesis. *Gb-gcl* transcripts were detectable at the
297 highest levels in the first eight hours after egg-lay (Figure 1B), suggesting maternal deposition of
298 *Gb-gcl* transcript. Consistent with this hypothesis, *Gb-gcl* transcript was detectable by *in situ*
299 hybridization in ovaries but not during embryogenesis (Supplemental Figure 1C–D).

300 Although we were unable to detect localized *gcl* expression in either *O. fasciatus* or *G.*
301 *bimaculatus* embryos, we still sought to determine whether the gene's documented roles in germ
302 cell specification (*D. melanogaster*) or adult spermatogenesis (*M. musculus*) might be conserved
303 (Jongens et al., 1992; Kimura et al., 2003). To this end, we analyzed *gcl* loss of function
304 conditions in embryos and adult gonads of both species. *gcl* is also required for transcriptional
305 quiescence in germ cells in *D. melanogaster* (Leatherman et al., 2002). However, we could not
306 detect any reduction in transcriptional activity in germ cells relative to somatic cells of either *O.*
307 *fasciatus* or *G. bimaculatus* (Supplemental Figure 2), so we did not assess this phenotype in our
308 functional studies of *gcl*.

309

310 *Of-gcl mutation decreases germ cell number in milkweed bug embryos.*

311 To determine whether *gcl* is required for germ cell specification in *O. fasciatus*, we
312 generated an *Of-gcl* putative protein-null allele with CRISPR/Cas9-mediated mutagenesis
313 (Figure 2A–B). This allele contains a 2-bp insertion at amino acid residue 14. The resulting
314 frameshift leads to a premature stop codon, resulting in a predicted peptide of 30 amino acid
315 residues, compared with the 478-residue wild type protein. Surprisingly, individuals homozygous
316 for this mutant allele were viable and fertile, and we have maintained a stable mutant line for at
317 least twelve generations at the time of writing. There were no detectable morphological defects
318 in adult ovaries or testes from this mutant line, nor any evidence of abnormal gametogenesis in
319 either males or females (Supplemental Figures 3–4).

320 In *O. fasciatus*, germ cells are first detectable in stage 3 on the interior of the cellular
321 blastoderm, forming part of an invaginating structure called the posterior pit (Ewen-Campen et
322 al., 2013b). The germ cells remain at the posterior end of the germ band as it forms by
323 invaginating into the egg (Ewen-Campen et al., 2013b) (Figure 2B; Supplemental Figure 5). At
324 stage 3, *gcl* mutant embryos had on average 35% fewer germ cells than wild type embryos ($p <$
325 0.001; $n = 14$ wild type, 8 *gcl* embryos; Figure 2C–D; Supplemental Table 2). Germ cell number
326 remained significantly lower in *gcl* mutant embryos relative to wild type embryos throughout all
327 embryonic stages examined (Figure 2D). We detected a marginal decrease in germ cell
328 proliferation in *gcl* mutant embryos relative to wild type only at stages 6 and 9, as measured by
329 the proportion of germ cells with detectable phospho-histone 3 (Figure 2E; Supplemental Table
330 2). However, there was no detectable difference in germ cell proliferation between the two
331 genotypes at any other embryonic stage examined (Figure 2E; Supplemental Table 2). We were

332 also unable to detect cleaved caspase 3-dependent cell death in stages 3–4 of either genotype (*n* =
333 27 wild type, 23 *gcl* embryos). Given that the discrepancy in germ cell number did not appear to
334 be the result of differences in cell proliferation or cell death, these data suggest that *Of-gcl* is
335 involved in, but not strictly necessary for, one or more of germ cell specification, formation or
336 maintenance.

337 In *D. melanogaster*, Gcl promotes germ cell fate by targeting the receptor Torso for
338 degradation, and *torso* RNAi in *gcl* mutant flies restores germ cell numbers to wild type levels
339 (Pae et al., 2017). To determine whether this mechanism of germ cell number determination is
340 conserved in *O. fasciatus*, we asked whether *torso* loss of function also affects germ cell number
341 in this species. Despite previous reports that the *O. fasciatus* genome lacks a *torso* ortholog
342 (Skelly et al., 2019; Weisbrod et al., 2013), we identified a high-confidence homolog in the
343 published genome assembly (Panfilio et al., 2019) (Figure 3A). Knockdown of *Of-torso* by
344 embryonic RNAi did not affect germ cell number in stages 3–4 in either wild type or *gcl* mutant
345 backgrounds (Figure 3B–C). This result suggests that the mechanism through which *gcl* controls
346 germ cell number is not conserved between *O. fasciatus* and *D. melanogaster*.

347

348 *Gb-gcl knockdown does not affect germ cell number in cricket embryos.*

349 To determine whether *gcl* is required for germ cell specification in *G. bimaculatus*, we
350 knocked down *gcl* expression using embryonic RNAi. We found no significant difference in total
351 germ cell number in stage 8 embryos under *gcl* knockdown relative to *gfp* control, nor did we
352 detect any significant difference in germ cell number in any segment (Figure 4). qPCR analysis
353 of injected embryos confirmed that RNAi was effective at reducing *gcl* transcript levels to 34%

354 relative to controls. It is possible that knockdown efficiency is not high enough with RNAi to
355 affect germ cell specification. However, we note that we have previously detected significant
356 changes in germ cell number with comparable or lower knockdown efficiencies (Barnett et al.,
357 2019; Donoughe et al., 2014; Nakamura and Extavour, 2016). Therefore, we speculate that the
358 role of *Gb-gcl* in germ cell specification or maintenance, if any, must be subtle.

359 Next, we asked whether *gcl* has any role in adult gametogenesis in *G. bimaculatus* by
360 performing RNAi in adult crickets. We could not detect any morphological or gametogenesis
361 defects in either ovaries or testes (Supplemental Figures 1–2). These data suggest that *gcl* is not
362 required for adult gametogenesis in this cricket.

363

364 **Discussion**.

365 Our analysis of *gcl* loss of function in embryos of two different hemimetabolous insects
366 suggests that *gcl* is not required for germ cell specification in these species, in contrast to the
367 gene's importance in germ cell formation in *D. melanogaster*. However, *Of-gcl* knockout
368 embryos have significantly fewer germ cells than wild type embryos, suggesting that the gene
369 may be involved in germ cell specification or maintenance in this bug, even if it is not strictly
370 required.

371 Gcl protein suppresses the somatic cell fate in *D. melanogaster* by targeting the receptor
372 tyrosine kinase Torso for degradation (Colonnetta et al., 2021; Pae et al., 2017). Germ cell
373 number can thus be modulated in flies by up- or downregulating Torso activity (Pae et al., 2017).
374 However, RNAi knockdown of *torso* in *O. fasciatus* does not affect germ cell number in either
375 wild type or *gcl* mutant embryos (Figure 3). Therefore, we hypothesize that germ cell

376 specification in this species does not require downregulation of Torso by Gcl, and that *Of-gcl*
377 regulates germ cell specification through some other unknown pathway. Torso's role in germ cell
378 specification may have been co-opted from its ancestral functions in neuroendocrine signaling,
379 just as it is thought to have been co-opted into its role in terminal patterning in flies (Duncan et
380 al., 2013; Schoppmeier and Schröder, 2005).

381 In *D. melanogaster*, the interaction between and Gcl and Torso proteins depends on
382 sequence motifs present on both proteins (Pae et al., 2017). In Gcl protein, this motif is the GCL
383 domain, which is conserved across insect homologs (Supplemental Figure 6) (Pae et al., 2017).
384 Torso interacts with Gcl through a motif in the linker domain between its split kinase domains.
385 This linker region is significantly longer in *Dm*-Torso compared with other insect homologs
386 (Supplemental Figure 7), and the specific motif identified by Pae and colleagues (Pae et al.,
387 2017) is not present in other homologs. The conservation of the GCL domain despite the lack of
388 conservation in the Torso interaction motif may suggest that Gcl has some other unknown
389 interaction partner, or that the Gcl–Torso interaction may not be as sequence-specific as
390 originally thought. AlphaFold3 (Abramson et al., 2024) predicts potential interaction between
391 Gcl and Torso homologs in both *O. fasciatus* and *G. bimaculatus* through the split kinase linker
392 domain of Torso (Supplemental Figure 8). Further experiments will be needed to test whether
393 these proteins interact *in vivo*, and to identify additional conserved interaction partners of Gcl.

394 In mice, *gcl* knockout results in abnormal nuclear morphology in the liver, pancreas and
395 testis, though the only functional defect identified was impaired spermatogenesis (Kimura et al.,
396 2003). Similarly, *gcl* is expressed at low levels in somatic tissues in flies including the gut,
397 muscle and nervous system, but no defects have been reported in those tissues in *gcl*-null flies
398 (Jongens et al., 1992; Robertson et al., 1999). We were also unable to detect any defects in

399 spermatogenesis under either *Of-gcl* knockout or *Gb-gcl* knockdown conditions (Supplementary
400 Figure 1). Given that the mouse *gcl* homolog can rescue germ cell formation in *gcl*-null flies
401 (Leatherman et al., 2000), its biochemical functions are likely to be conserved across these
402 species. We speculate that *gcl* has a ubiquitous but subtle cell biological role in maintaining
403 nuclear morphology that only yields a phenotype in certain tissue contexts, such as in mouse
404 spermatogenesis. Under this hypothesis, *gcl* then gained an additional role in germ cell
405 specification in certain lineages of insects. In addition, the mechanism underlying this germ cell
406 specification has diverged between insect lineages, perhaps through the evolution of new
407 interaction partners such as Torso. This model reflects the complexity and variation present in the
408 mechanisms of germ cell specification and their evolution, including the co-option of new genes
409 with the shifting mechanisms of this process across animals.

410

411 **Author contributions**

412 JAK: Conceptualization, Methodology, Formal Analysis, Investigation, Writing – Original Draft,
413 Writing – Review & Editing, Visualization; CGE: Conceptualization, Writing – Review &
414 Editing, Supervision, Funding Acquisition

415

416 **Acknowledgments**

417 The authors thank members of the Extavour lab for valuable discussions. This research was
418 supported by National Science Foundation (NSF) Awards IOS-2220747 and IOS-0817678 to
419 CGE, and an NSF Graduate Research Fellowship to BE-C.

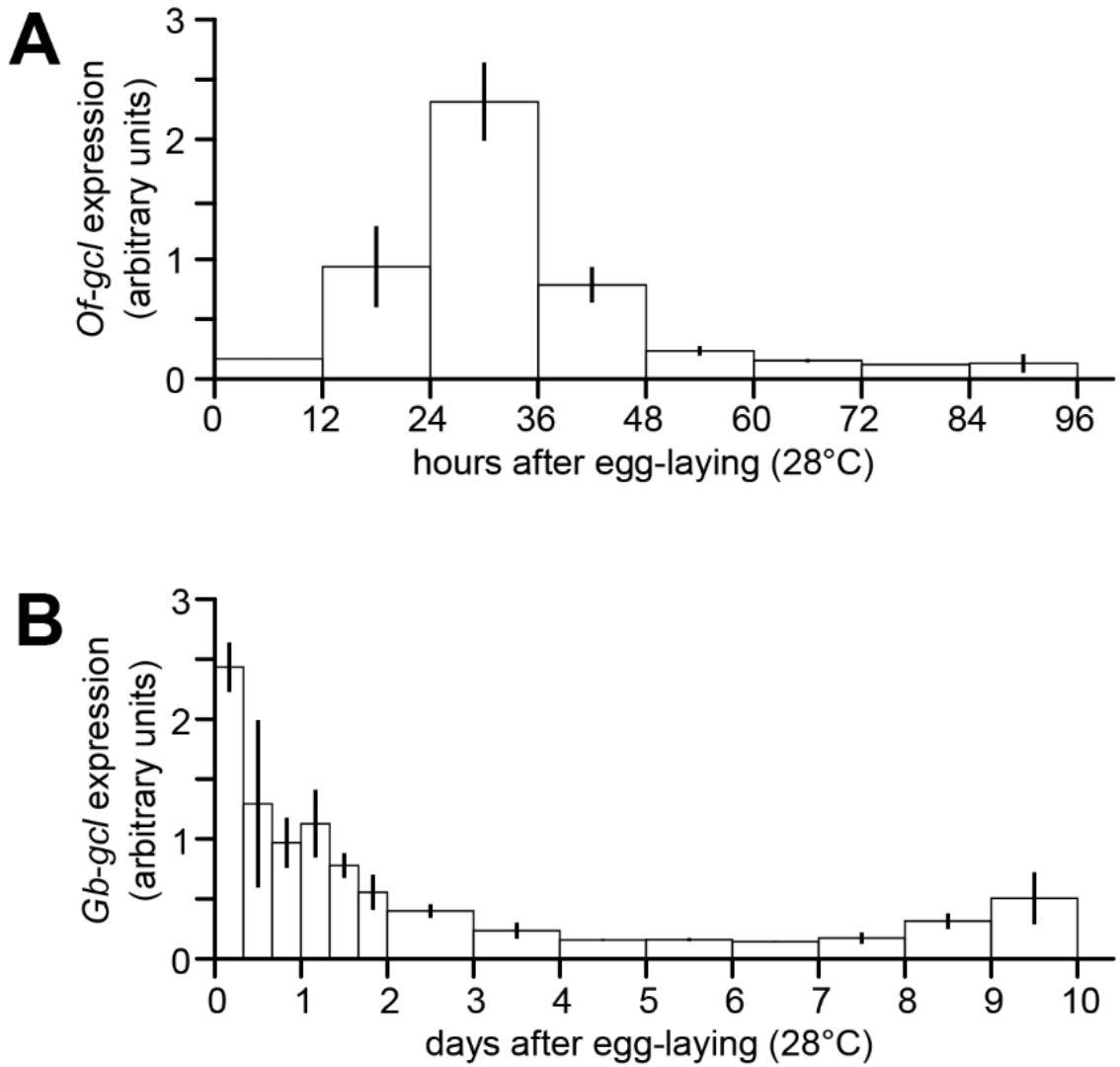

420

421 **Figure 1. *gcl* expression is detectable by qPCR in *O. fasciatus* (A) and *G. bimaculatus* (B) embryos.** C_q values were normalized
422 against *Of-gapdh* or *Gb-tubulin* expression and averaged over four biological replicates for each time point. Error bars represent
423 standard deviations. The width of each bar represents the length of time for each embryo collection.

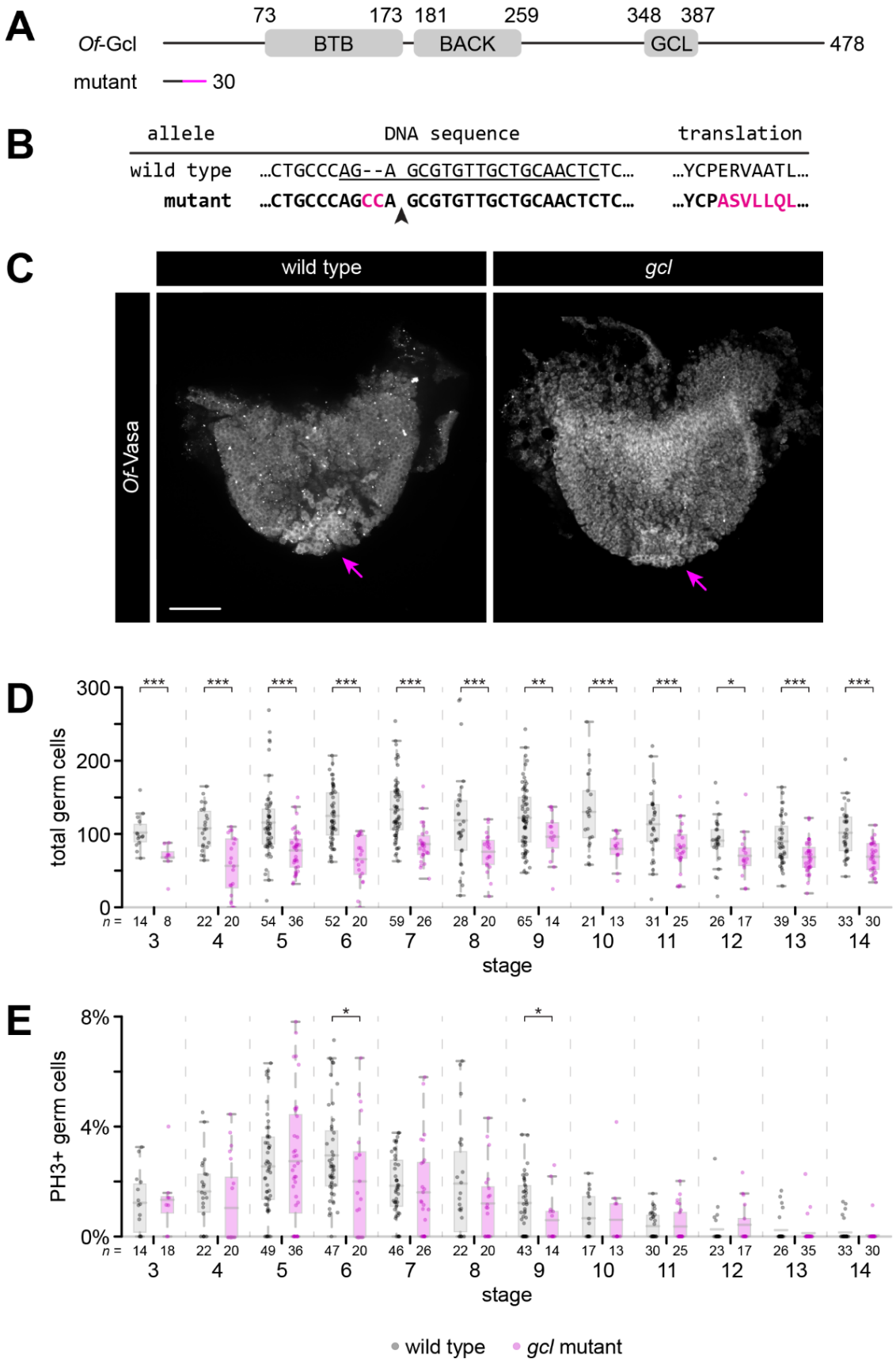
A
Of-Gcl
73
173
181
259
348
387
478
BTB
BACK
GCL
mutant
30
B
allele
DNA sequence
translation
wild type
…CTGCCCAG--A GCGTGTTGCTGCAACTCTC…
…YCPERVAATL…
mutant
…CTGCCCAGCCA GCGTGTTGCTGCAACTCTC…
…YCPASVLLQL…
C
wild type
gcl
Of-Vasa
D
total germ cells
stage
E
PH3+ germ cells
stage
wild type
gcl mutant

425 **Figure 2 (previous page). *Of-gcl* mutation decreases germ cell number in embryos.**

426 (**A**) Predicted domain architecture of *Of*-Gcl and predicted mutant protein. Wild type *Of*-Gcl has
427 two predicted folded domains (BTB and BACK domains) as well as a conserved motif called the
428 GCL domain. The predicted mutant protein contains none of these domains and is truncated after
429 residue 30.

430 (**B**) *Of-gcl* mutant allele contains a two base pair insertion, creating a frameshift and leading to a
431 predicted truncated protein. Guide sequence is underlined; arrowhead marks predicted Cas9 cut
432 site. Inserted bases and predicted mutated residues are indicated in magenta.

433 (**C**) Representative antibody stains against *Of*-Vasa to mark germ cells in stage 3 wild type and
434 *gcl* mutant embryos. Mutant embryos still have germ cells at the expected location, indicated by
435 arrows. Scale bar = 100 µm.

436 (**D**) Germ cell counts across embryogenesis in wild type and *gcl* mutant embryos. Mutant
437 embryos have significantly fewer germ cells per embryo compared to wild type.

438 (**E**) Proportion of $PH3^+$ germ cells across embryogenesis in wild type and *gcl* mutant embryos.
439 There is no significant difference in the proportion of proliferating germ cells between wild type
440 and *gcl* mutant embryos.

441 All statistical tests are non-parametric bootstrap comparisons. Embryonic stages are defined in
442 Supplemental Figure 5 and Supplemental Table 3. * $p < 0.05$; ** $p < 0.01$; *** $p < 0.001$

443

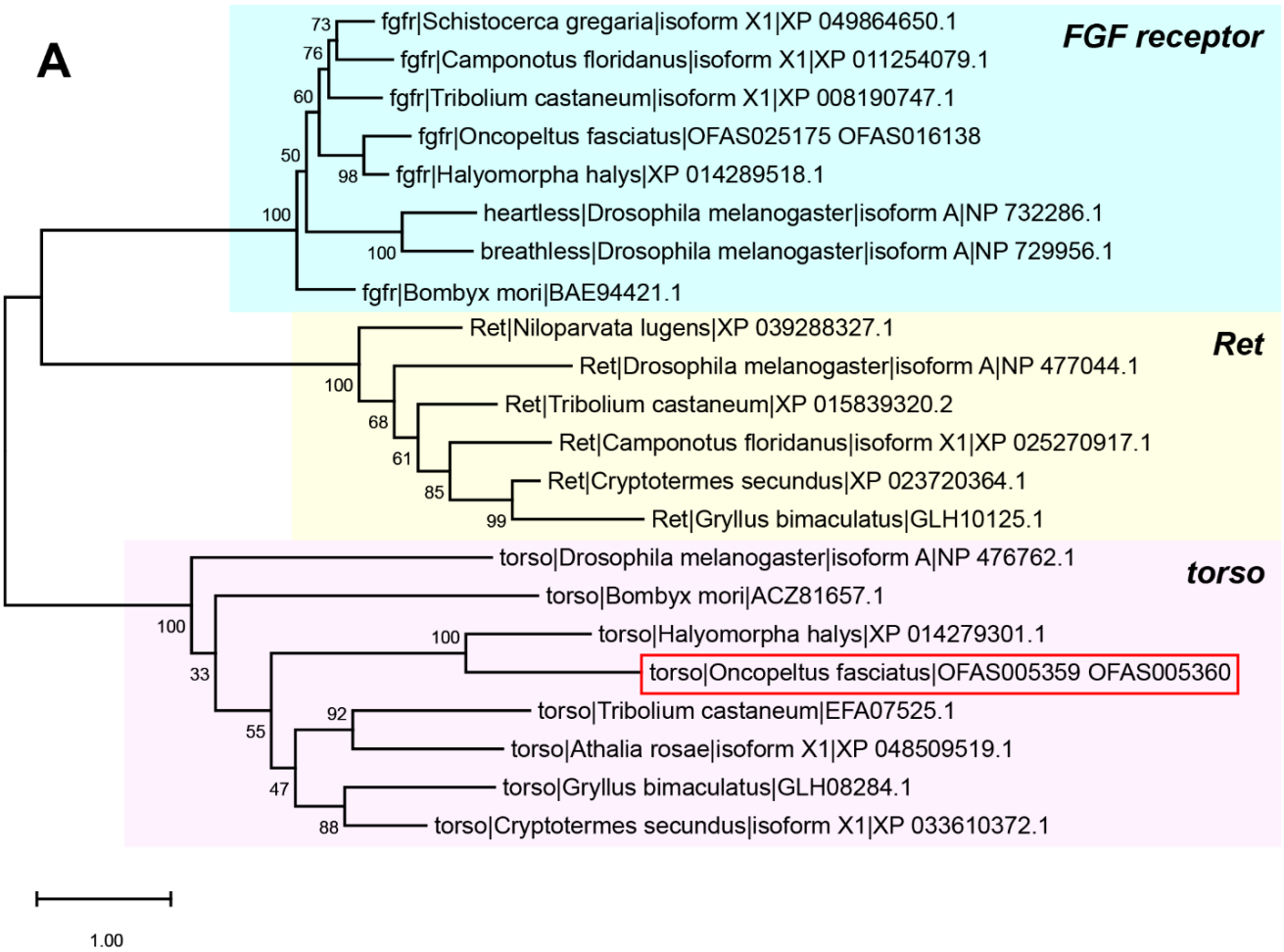
A
FGF receptor
fgfr|Schistocerca gregaria|isoform X1|XP 049864650.1
fgfr|Camponotus floridanus|isoform X1|XP 011254079.1
fgfr|Tribolium castaneum|isoform X1|XP 008190747.1
fgfr|Oncopeltus fasciatus|OFAS025175 OFAS016138
fgfr|Halyomorpha halys|XP 014289518.1
heartless|Drosophila melanogaster|isoform A|NP 732286.1
breathless|Drosophila melanogaster|isoform A|NP 729956.1
fgfr|Bombyx mori|BAE94421.1
Ret
Ret|Niloparvata lugens|XP 039288327.1
Ret|Drosophila melanogaster|isoform A|NP 477044.1
Ret|Tribolium castaneum|XP 015839320.2
Ret|Camponotus floridanus|isoform X1|XP 025270917.1
Ret|Cryptotermes secundus|XP 023720364.1
Ret|Gryllus bimaculatus|GLH10125.1
torso
torso|Drosophila melanogaster|isoform A|NP 476762.1
torso|Bombyx mori|ACZ81657.1
torso|Halyomorpha halys|XP 014279301.1
torso|Oncopeltus fasciatus|OFAS005359 OFAS005360
torso|Tribolium castaneum|EFA07525.1
torso|Athalia rosae|isoform X1|XP 048509519.1
torso|Gryllus bimaculatus|GLH08284.1
torso|Cryptotermes secundus|isoform X1|XP 033610372.1
1.00

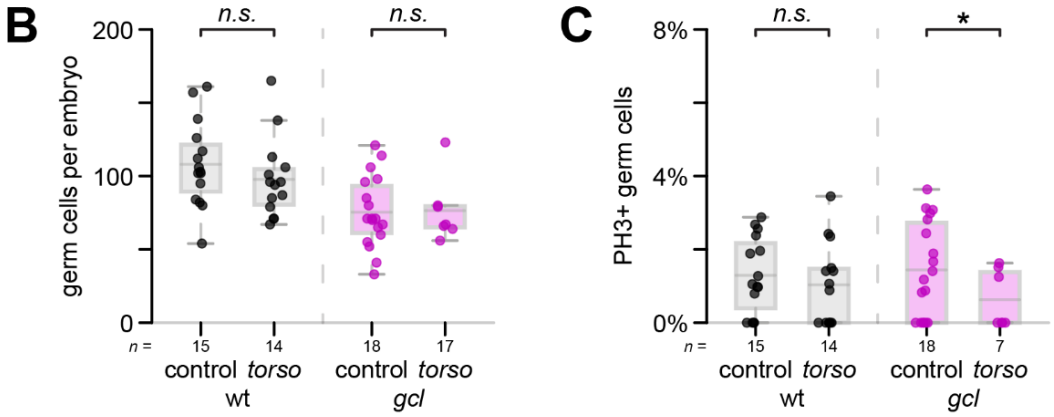
B
germ cells per embryo
n.s.
n.s.
n =
control torso
wt
control torso
gcl
C
PH3+ germ cells
n.s.
*

444

445

446 **Figure 3 (previous page). *Of-torso* knockdown does not affect embryonic germ cell number.**

447 (**A**) Phylogenetic analysis of *torso* and related receptor tyrosine kinases (*Ret oncogene* and *FGF*
448 *receptor*) across insects. Each clade is individually highlighted for clarity. The putative *torso*
449 homolog from *O. fasciatus* (OFAS005359/OFAS0005360) falls within the *torso* clade.

450 (**B**) Germ cell counts in stage 3–4 *Of-torso* RNAi embryos, performed in wild type and *gcl*
451 mutant backgrounds. *torso* knockdown does not affect germ cell number in either background.

452 (**C**) Proportion of $PH3^+$ germ cells in stage 3–4 *Of-torso* RNAi embryos, performed in wild type
453 and *gcl* mutant backgrounds. *torso* knockdown marginally reduces germ cell proliferation in *gcl*
454 mutant embryos but not in wild type embryos.

455 All statistical tests are non-parametric bootstrap comparisons.
456 * $p < 0.05$; ** $p < 0.01$; *** $p < 0.001$

457

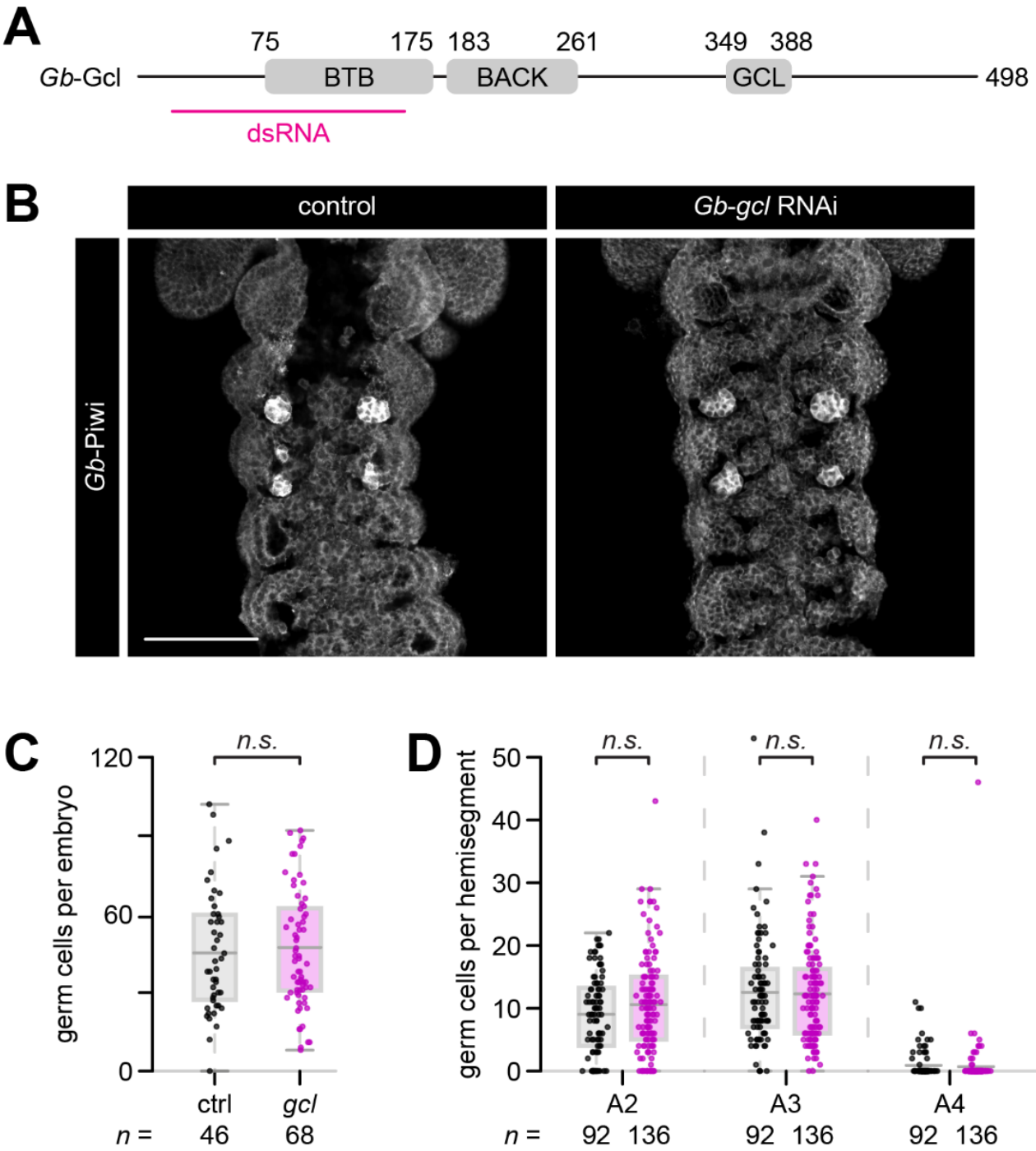
A
75
175
183
261
349
388
Gb-Gcl
BTB
BACK
GCL
498
dsRNA
B
control
Gb-gcl RNAi
Gb-Piwi
C
n.s.
germ cells per embryo
120
60
0
ctrl
gcl
n =
46
68
D
n.s.
n.s.
n.s.
germ cells per hemisegment
50
40
30
20
10
0
A2
A3
A4
n =
92
136
92
136
92
136

458

459

460 **Figure 4 (previous page). *Gb-gcl* knockdown does not affect embryonic germ cell number.**

461 (**A**) Predicted domain architecture of *Gb*-Gcl. *Gb*-Gcl has two predicted folded domains (BTB
462 and BACK domains) and a conserved motif called the GCL domain. The fragment region used
463 for dsRNA synthesis is marked.

464 (**B**) Representative antibody stains against *Gb*-Piwi to mark germ cells in stage 8 control and *gcl*
465 knockdown embryos. Embryos in which *Gb-gcl* has been knocked down still have germ cells in
466 the expected positions. Scale bar = 100 µm.

467 (**C**) Germ cell counts in stage 8 *Gb-gcl* RNAi embryos. Germ cell numbers are not significantly
468 different in *Gb-gcl* knockdown embryos relative to control. Each point represents one embryo.

469 (**D**) Germ cell counts in stage 8 *Gb-gcl* RNAi embryos, divided into hemisegments (*i.e.*, the left
470 or right half of one segment). *Gb-gcl* knockdown does not affect the number of germ cells in any
471 individual segment. Each point represents a hemisegment.

472 All statistical tests are non-parametric bootstrap comparisons.

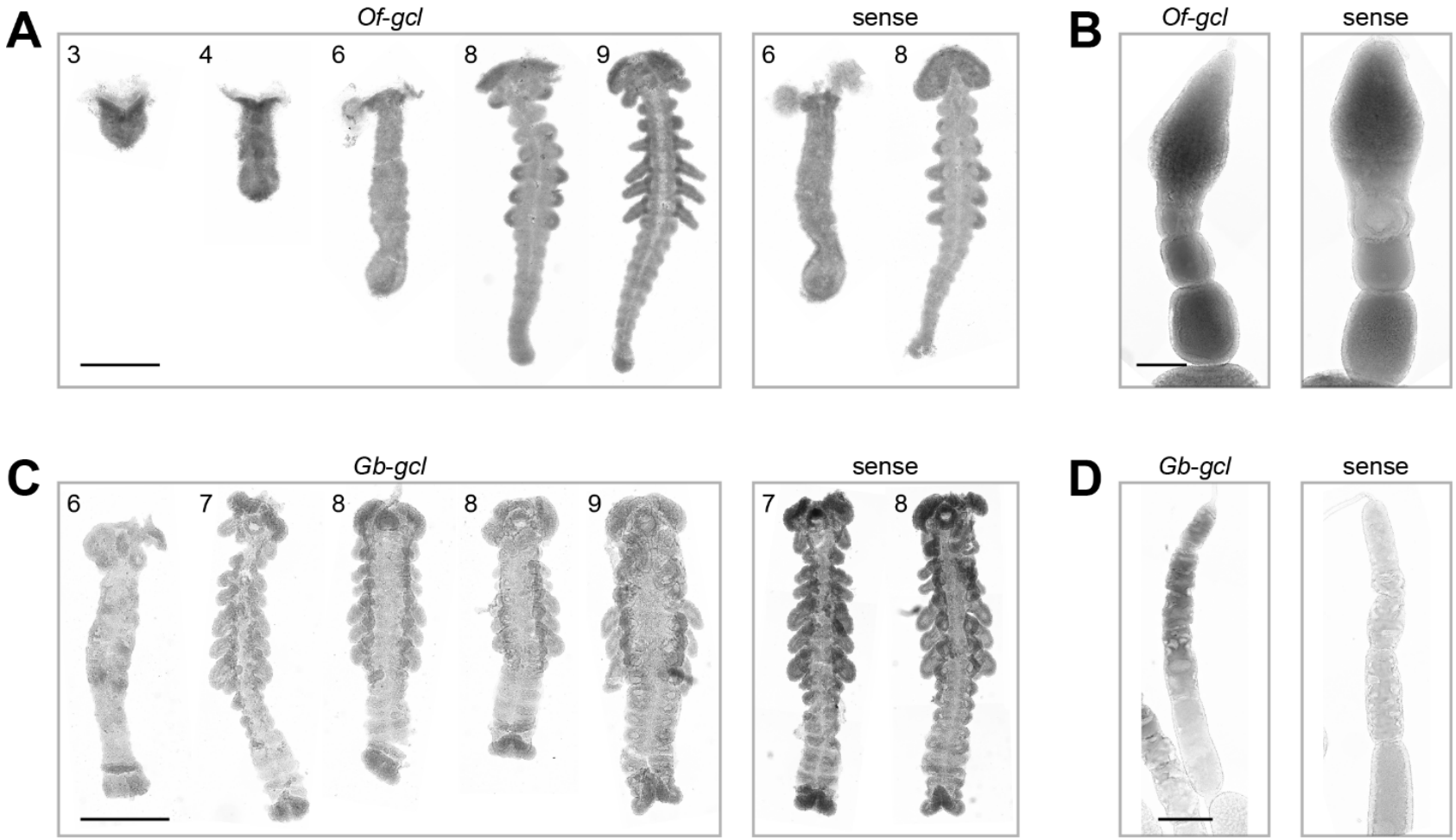

Supplemental Figure 1. *gcl* is not detectable with *in situ* hybridization during embryogenesis in *O. fasciatus* or *G. bimaculatus*.

(**A**–**B**) *In situ* hybridization against *Of-gcl* in embryos (C) and ovaries (D). Numbers indicate embryonic stages. Scale bars = 500 µm (embryos) or 200 µm (ovaries).

(**C**–**D**) *In situ* hybridization against *Gb-gcl* in embryos (E) and ovaries (F). Numbers indicate embryonic stages. Scale bars = 500 µm (embryos) or 200 µm (ovaries).

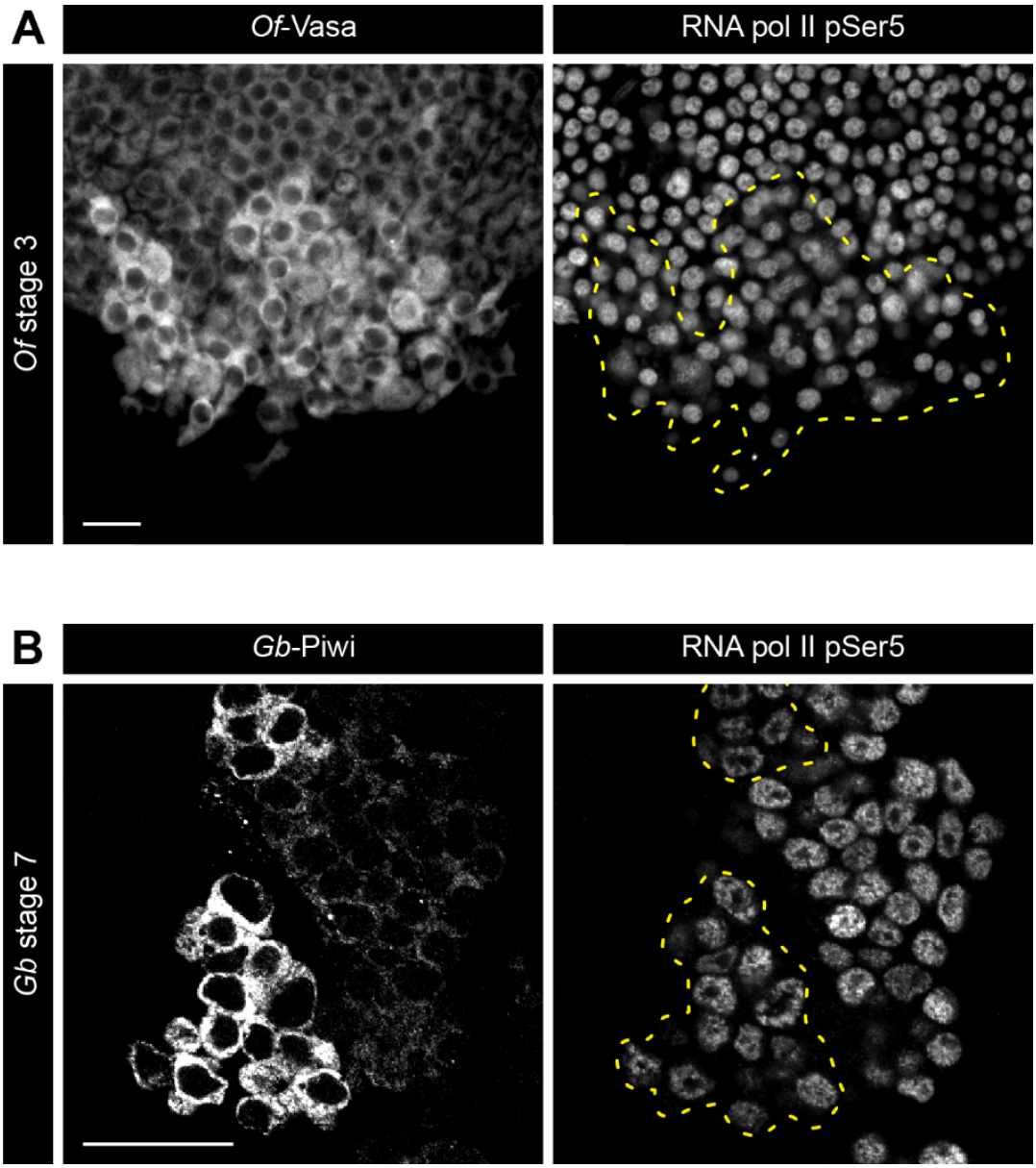

Supplemental Figure 2. Germ cells in *O. fasciatus* and *G. bimaculatus* are not transcriptionally quiescent.

(**A**) Antibody stains in stage 3 *O. fasciatus* embryos against *Of*-Vasa to visualize germ cells and against hyperphosphorylated RNA polymerase II to visualize transcriptional activity. Germ cells are transcriptionally active. Scale bar = 25 µm.

(**B**) Antibody stains in stage 7 *G. bimaculatus* embryos against *Gb*-Piwi to visualize germ cells and against hyperphosphorylated RNA polymerase II to visualize transcriptional activity. Germ cells are transcriptionally active. Scale bar = 25 µm.

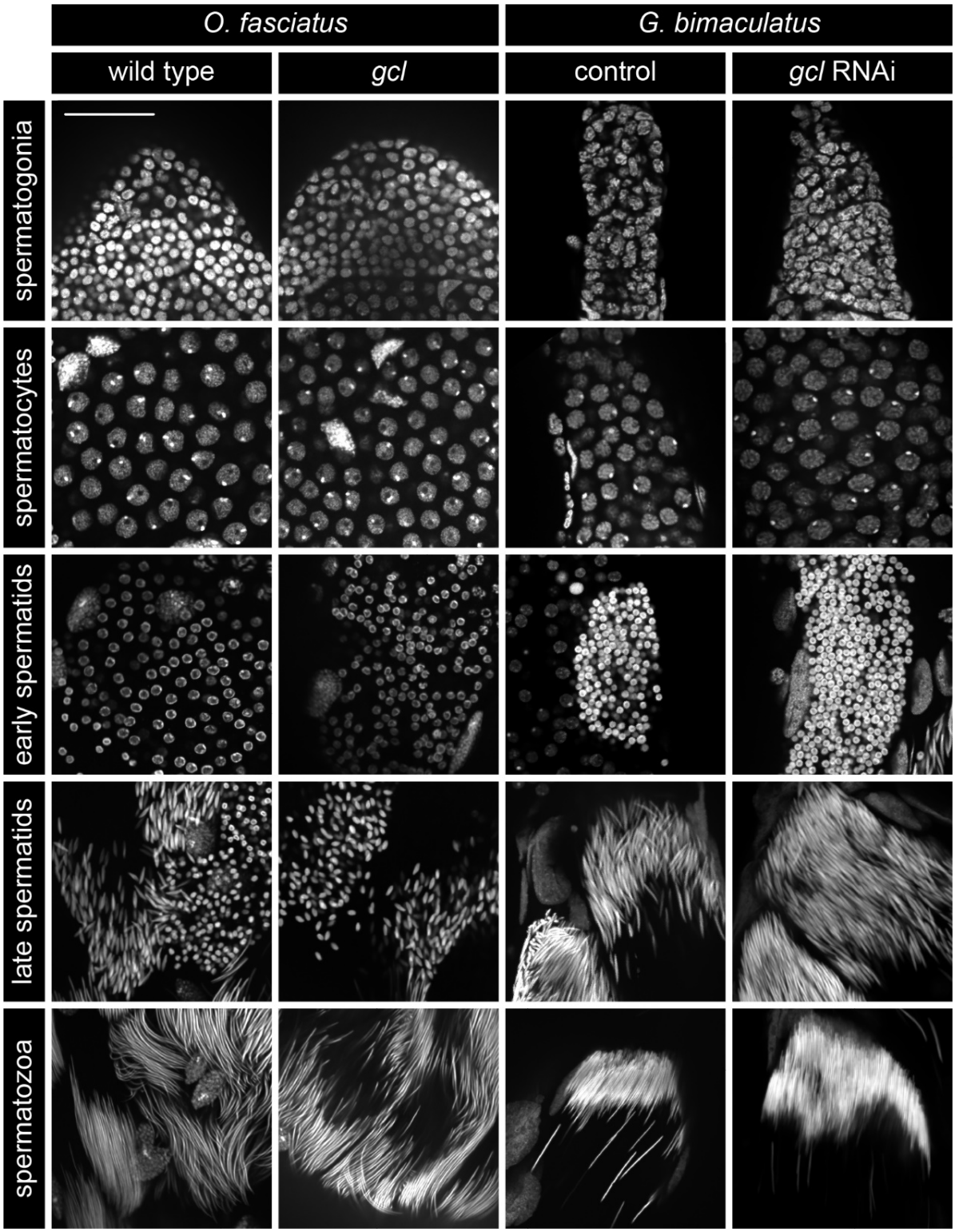

Supplemental Figure 3. Lack of *gcl* activity does not affect the progression of adult spermatogenesis in either *O. fasciatus* or *G. bimaculatus*. Representative images of Hoechst-stained testes showing different stages of spermatogenesis in both species under both wild type and *gcl* loss of function conditions. Scale bar = 50 µm.

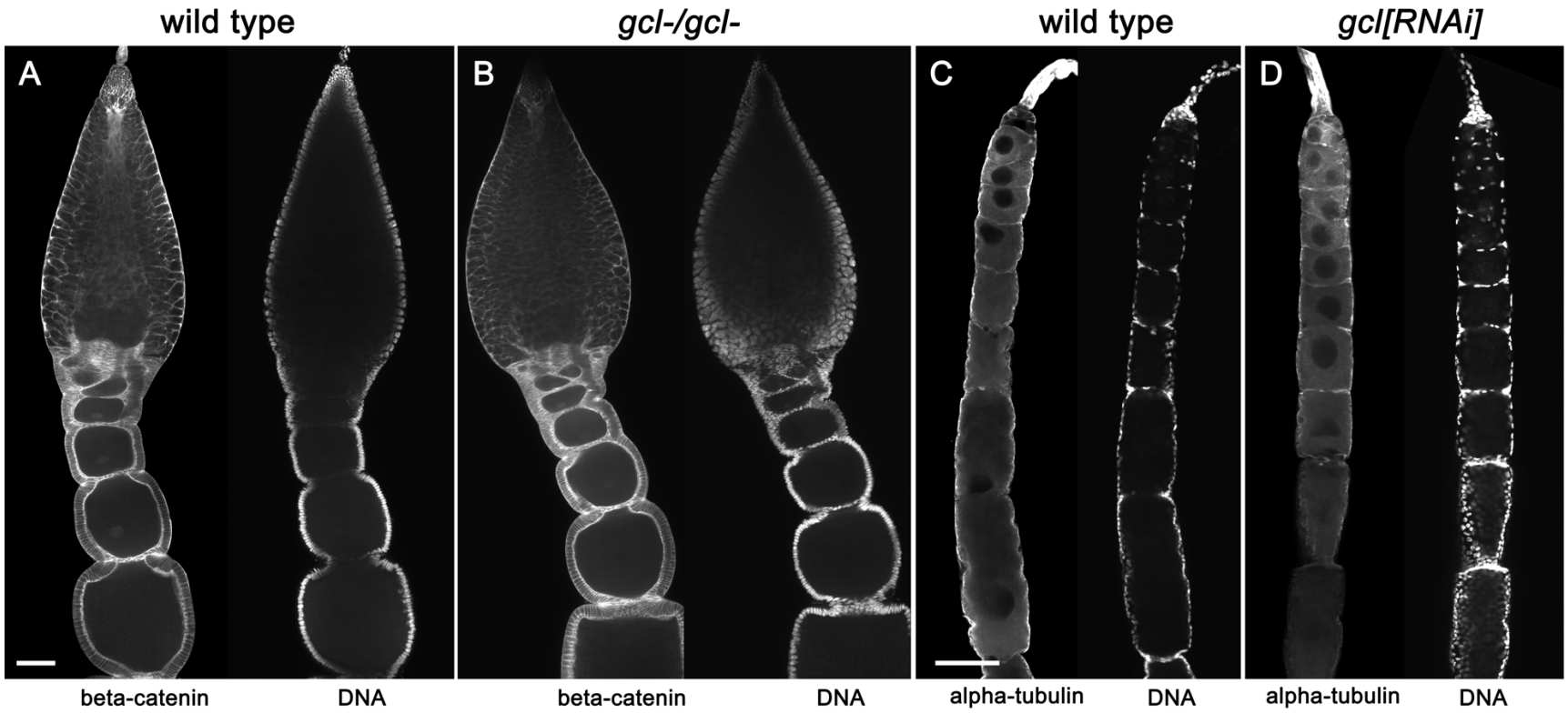

Supplemental Figure 4. Lack of *gcl* activity does not affect adult oogenesis in either *O. fasciatus* or *G. bimaculatus*. Representative images of single 1 µm optical sections of ovarioles under both wild type ((A) *O. fasciatus*; (C) *G. bimaculatus*) and (B) *gcl* knockout (*O. fasciatus*) or (D) knockdown (*G. bimaculatus*) conditions. Scale bars = 100 µm in (A) (applies also to (B)) and (C) (applies also to (D)).

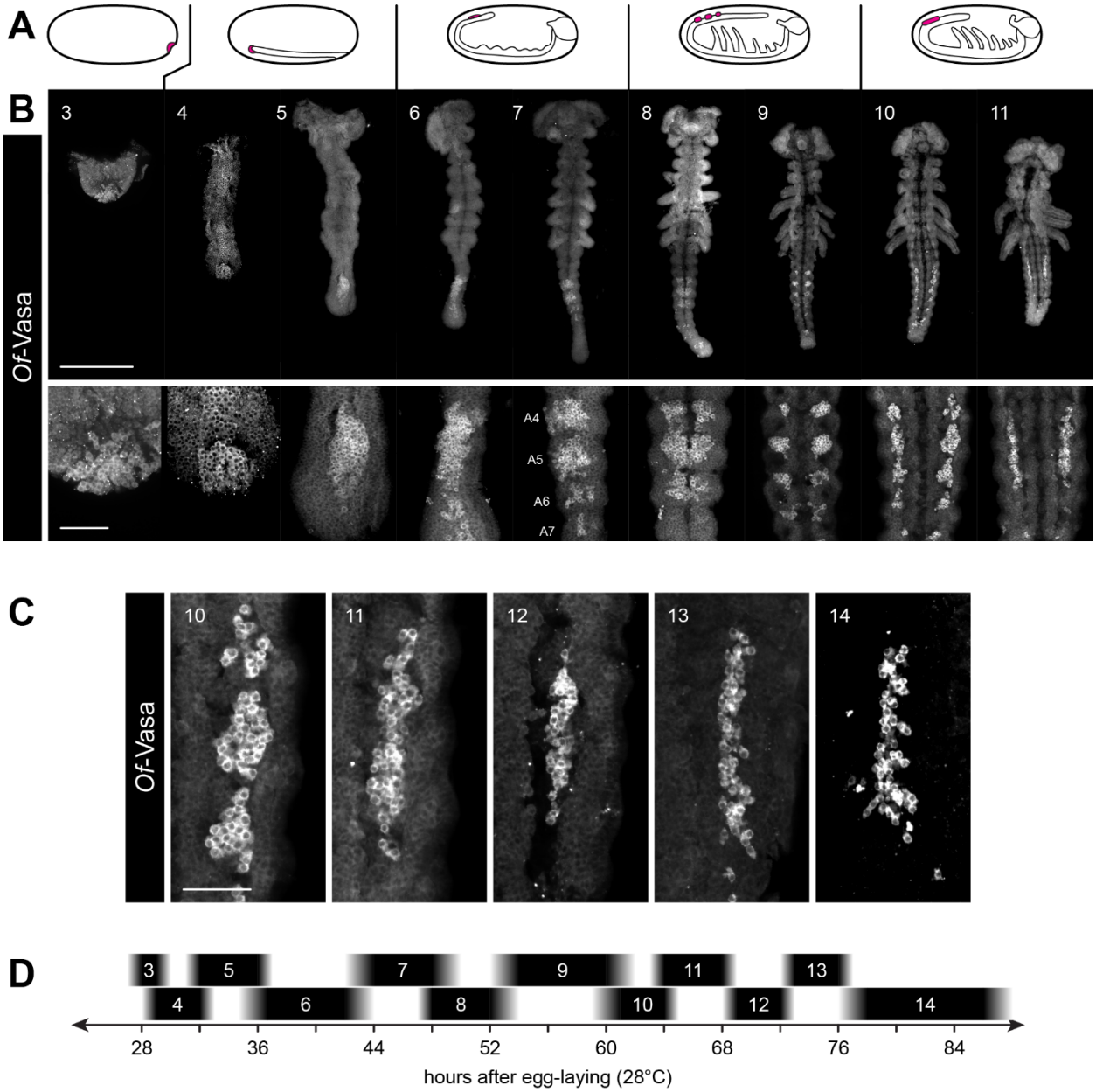

Supplemental Figure 5. Wild type germ line development in *O. fasciatus*.

(**A**) Schematics showing the position of the *O. fasciatus* embryo within the egg, roughly corresponding to the stages shown below in (**B**). Germ cells are indicated in magenta.

(**B**) Representative images of *Of*-Vasa antibody stains in stage 3–11 *O. fasciatus* embryos. Top row shows whole mount embryos, while the bottom row shows a higher magnification view of the germ cells. Scale bar = 500 µm in top row, 100 µm in bottom row.

(**C**) *Of*-Vasa antibody stains in stages 10–14 showing coalescence of germ cells into the embryonic gonad. Right gonad shown in all images. Scale bar = 50 µm.

(**D**) Timeline of embryonic stages for wild type development at 28°C, 60% humidity.

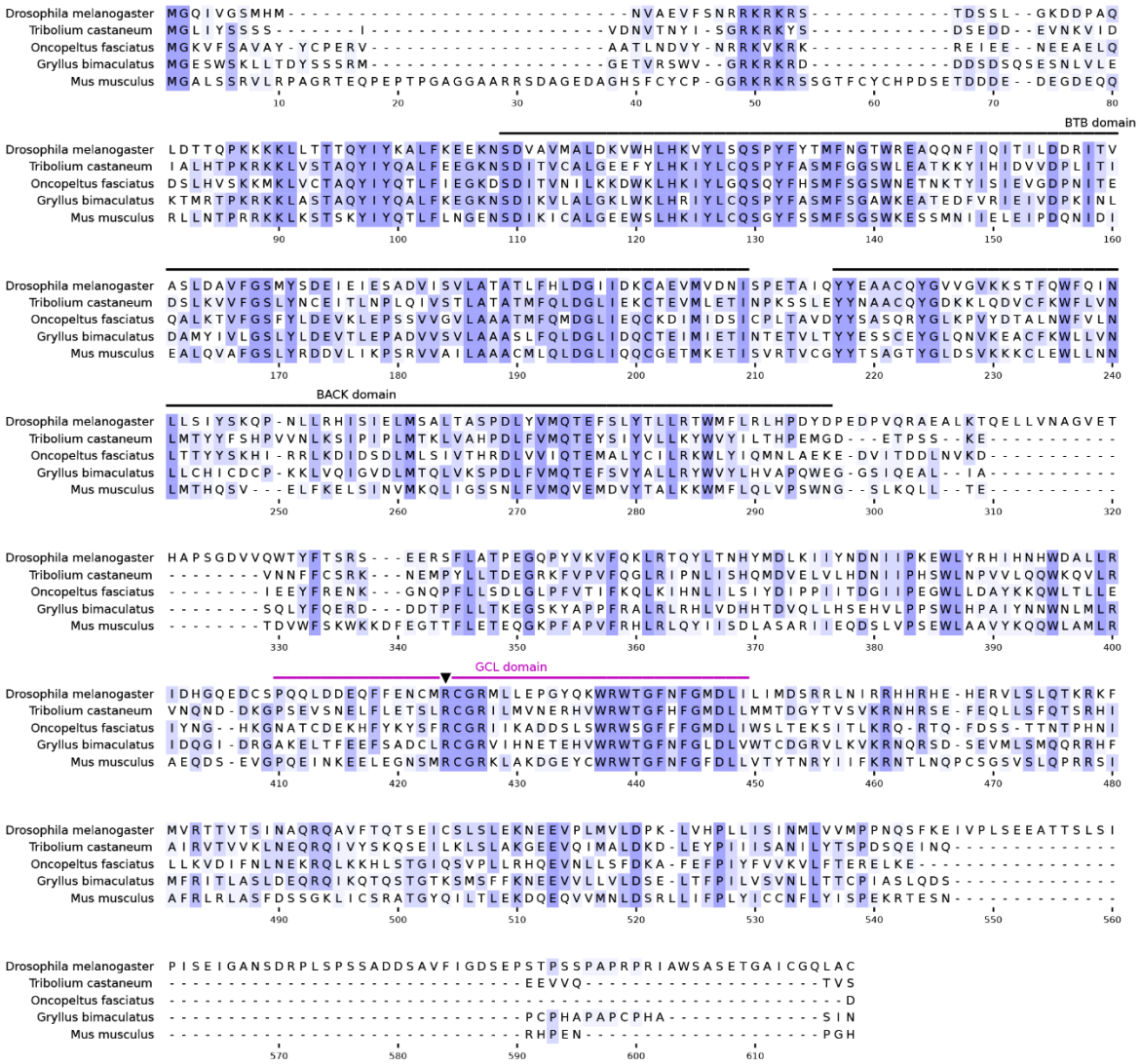

Supplemental Figure 6. MUSCLE alignment of select *gcl* homologs. Darker shading represents greater degree of conservation at each position. The conserved GCL domain identified by Pae and colleagues (Pae et al., 2017) is marked in magenta. In that study, the role of the GCL domain was directly tested by mutating the residue marked by the arrowhead (R377).

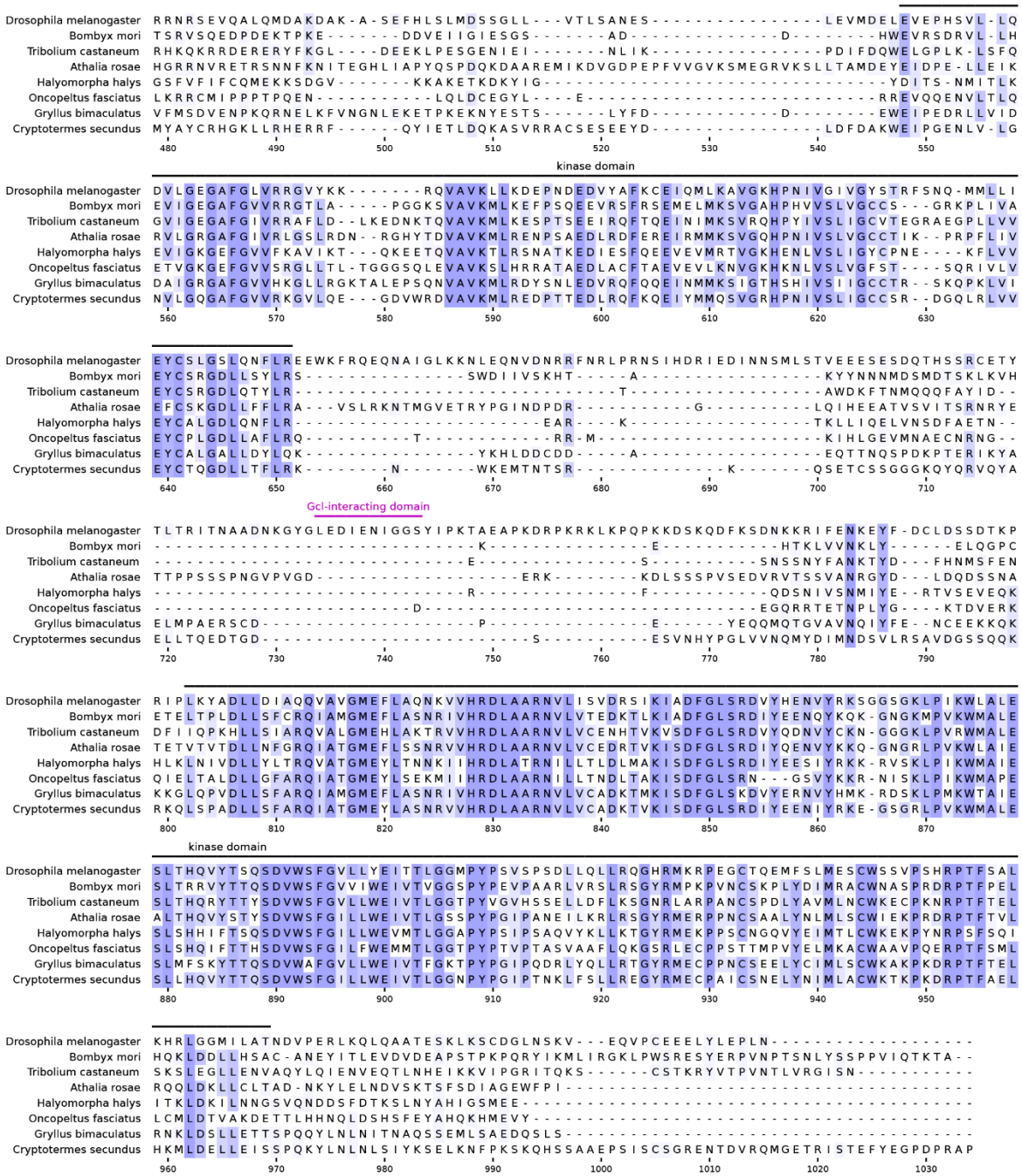

Supplemental Figure 7. MUSCLE alignment of the intracellular domain of select insect *torso* homologs. Darker shading represents greater degree of conservation at each position. The Gcl-interacting motif identified by Pae and colleagues (Pae et al., 2017) is marked in magenta. Note that this motif is not conserved in other insects; the surrounding domain is much longer in *D. melanogaster* compared with other homologs.

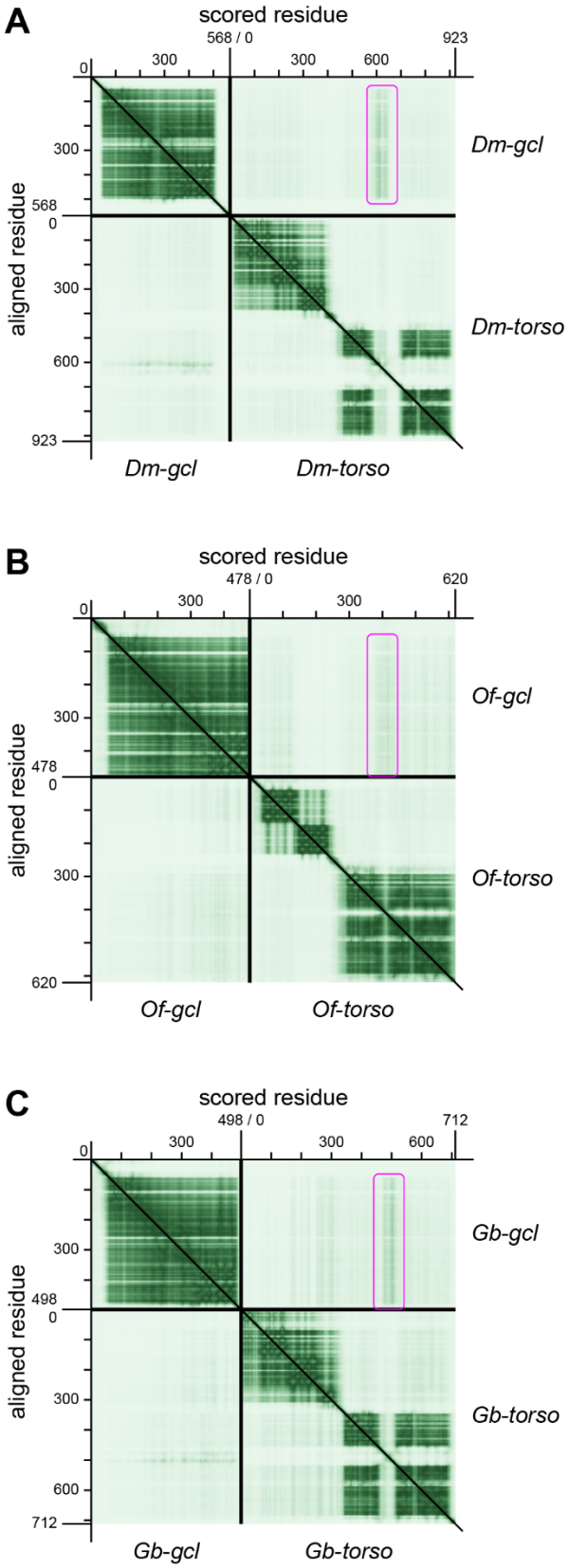

Supplemental Figure 8. AlphaFold3 predicts potential interactions between Gcl and Torso homologs. Predicted alignment error plots are shown for AlphaFold3 structure predictions of Gcl and Torso homologs from *D. melanogaster* (**A**), *O. fasciatus* (**B**) and *G. bimaculatus* (**C**). Darker color represents higher confidence (lower predicted error) in the relative positions of the scored and aligned residues. Overall confidence in the structure of the Gcl–Torso complex is low for all species. However, in all species, there is a region of Torso protein (marked in magenta) for which its predicted alignment error with Gcl is lower, suggesting a potential interaction between the two proteins through this region of Torso.

Supplemental Table 1. Primers used.

gene	direction	primer sequence	expected length
full-length sequence			
Of-gcl	forward	ATGGGTAAAGTATTCAGTGCAGTTGCT	1437 bp
	reverse	TTAGTCTTCTTTTAATTCTCTCTCTGTAAATAG	
Gb-gcl	forward	CGTCGATGAGCTAGTTGAGAGCTGA	1804 bp
	reverse	AGATGTTCAAGCATAGCCGCCCAAG	
in situ probe and dsRNA			
Of-gcl	forward	GCAGTTGCTTATTACTGCCCAGAGCGT	441 bp
	reverse	TGCAGCAGCCAGCACACCAACAACA	
Of-torso	forward	TCGAGGTCGCCGTCAAATCCCT	665 bp
	reverse	GGCAACAGACGCTGTCGGAACA	
Gb-gcl	forward	TGTCCGCTCGTGGGTCGGCAGAAAA	413 bp
	reverse	ACAGAGAGGCTGCAGCAAGCACTGA	
qPCR			
Of-gcl	forward	TCCAGAAGGTTGGTTGCTCGATGCCT	257 bp
	reverse	TGCTGCTGTCAAACTGTGTACGCTGCC	
Of-torso	forward	TGAGCATGGTGGGCGATTGCTG	288 bp
	reverse	AGGGATTTGACGGCGACCTCGA	
Gb-gcl	forward	GCACCACCATTTCGTGCACTTCGCC	258 bp
	reverse	ACCTGTCCATCGCCACACATGTTCT	
Of-gapdh	forward	TGGCAAACTAACTGGCATGGCA	171 bp
	reverse	ACAACCTGGTCATCAGTGTACGCCA	
Gb-β-tubulin	forward	TGGACTCCGTCCGGTCAGGC	166 bp
	reverse	TCGCAGCTCTCGGCCTCCTT	
RACE			
Of-torso	forward 1 (3' RACE)	ACTGGAGGAGGCTCCCAACTCGAGGTCGCC	
	forward 2 (3' RACE)	ACAGGAGGGCCACGGCAGAGGACTTGGCTT	
	reverse 1 (5' RACE)	TGGAGAAAGGCGGCAACAGACGCTGTCGGA	
	reverse 2 (5' RACE)	CGCTGGGAGGTAGAGAAGCCGACCAGGGAG	
Of-fgfr	forward 1 (3' RACE)	AACAAGGGCATACAGATGCAGAAATGACTG	
	forward 2 (3' RACE)	GCATCGGCCATCATCTGGTTATGAACCTGC	
	reverse 1 (5' RACE)	TATTCCTTGCTGCCAGGTCTCGATGTAAAC	
	reverse 2 (5' RACE)	TGACAGGTATTCCATGCCTCTAGCAACTTG	

Supplemental Table 2. Quantification of germ cell development in wild type and *gcl* mutant *O. fasciatus* embryos. All *p*-values were calculated using a non-parametric bootstrap test.

	total germ cells per embryo						proportion of PH3+ germ cells per embryo				
	wild type		*gcl*				wild type		*gcl*		
stage	mean	*n*	mean	*n*	ratio	*p*-value	mean	*n*	mean	*n*	*p*-value
3	102.00	14	68.13	8	0.668	<0.001	0.0126	14	0.0110	8	0.4221
4	108.00	22	56.55	20	0.524	<0.001	0.0181	22	0.0124	20	0.0953
5	115.69	54	77.58	36	0.671	<0.001	0.0221	49	0.0279	36	0.3386
6	124.71	52	65.70	20	0.527	<0.001	0.0250	47	0.0236	20	0.0382
7	133.54	59	86.19	26	0.645	<0.001	0.0137	46	0.0143	26	0.2572
8	118.57	28	75.70	20	0.638	<0.001	0.0108	22	0.0132	20	0.0745
9	122.19	65	96.36	14	0.789	0.002	0.0081	43	0.0067	14	0.0164
10	130.24	21	79.77	13	0.612	<0.001	0.0040	17	0.0058	13	0.4213
11	113.36	31	80.52	25	0.710	0.001	0.0040	30	0.0045	25	0.4566
12	91.04	26	70.29	17	0.772	0.017	0.0030	23	0.0042	17	0.2247
13	89.95	39	68.63	35	0.763	<0.001	0.0014	26	0.0012	35	0.1769
14	101.67	33	69.03	30	0.679	<0.001	0.0015	33	0.0005	30	0.0605

Supplemental Table 3. Staging table for wild type *O. fasciatus* embryogenesis at 28°C.

stage	hours ael (28°C)	stage description	germ cell development
1		Freshly laid egg.	
2		Uniform blastoderm.	
3	26–28	An indentation appears at the posterior end of the egg, called the posterior pit.	Primordial germ cells are first observed just inside the posterior pit, but we cannot currently perform antibody stains at this stage.
4	28–32	The germ band has invaginated into the posterior pit and extends toward the anterior. The orientation of the germ band is reversed with respect to the egg, *i.e.*, the posterior end of the germ band is closer to the anterior of the egg.	Primordial germ cells remain in a cluster at the posterior tip of the germ band. The Vasa antibody stain is inconsistent at this stage.
5	32–36	The thorax region is wider than the abdomen region (mediolaterally), but limb buds are not yet distinct. Segments have been specified up to A5–A7 but are not yet distinguishable without staining for a segmentation marker.	Germ cells are located in the bulbous part of the germ band, primarily in A5–A6, but with some in A4 and A7.
6	36–44	Limb buds are now distinct semicircles. Segments have been specified up to A7–A9 but are not yet distinguishable without staining for a segmentation marker.	Germ cells are located in a single cluster primarily in A4–A6, with some in A7. Segments in which germ cells are located are narrower in the medial–lateral axis compared with the posterior tip.
7	42–50	Segments start to become visibly distinct in the anterior abdomen around the time A9 is specified. Posterior tip is still round. Neural groove has formed at most up to A3.	Germ cells separate into segmental clusters. When there are many germ cells, they may still appear as one large medial cluster, especially as one spanning both segments A4 and A5.
8	48–54	Legs and gnathal appendages are triangular rather than semicircular lobes. A11 starts to thicken but the posterior tip is still mostly round.	Germ cells split into bilateral clusters as the neural groove forms in each segment. In this stage, germ cells are located right at the edges of the neural groove. When there are many germ cells in a particular segment, they may still appear to be one large medial cluster in that segment.
9	52–64	Neural groove has formed up to A8–A9. “Coelomic cavities” are visible as pits in all abdominal segments up to A9, though they may sometimes be obscured by germ cells, especially in A4–A6. Posterior end has folded over to form the proctodeum. Lateral	Germ cells have moved laterally away from the neural groove and clusters usually appear rounder.

		margins of the germ band are thickening in the gnathal and thoracic segments.	
10	60–64	Lateral margins of the germ band are thickening in the abdomen. Ganglia appear as two parallel rectangles in each segment, separated by the median cord along the midline. “Coelomic cavities” are no longer distinct.	Germ cell clusters lengthen along the AP axis and narrow along the medial–lateral axis. Adjacent clusters may fuse, but a segmental grouping is still visible.
11	64–68	Median cord clusters appear at segmental boundaries, and the ganglionic masses are now slightly crooked.	Germ cells are lined up in the genital ridges on each side of the embryo, parallel to the AP axis.
12	68–72	Abdominal cross commissures have formed. With a nuclear stain, ganglia appear as pairs of half circles facing away from each other.	Germ cells remain in the genital ridges.
13	72–76	The lateral cords move dorsolaterally and become parallel with the median cord again. Gonadal follicle primordia become visible in the nuclear channel.	Germ cells remain in the genital ridges.
14	76–	The embryo undergoes katatrepsis and begins dorsal closure. This stage will likely be subdivided further.	Germ cells start to migrate laterally into gonadal follicle primordia.

References

Abramson, J., Adler, J., Dunger, J., Evans, R., Green, T., Pritzel, A., Ronneberger, O., Willmore, L., Ballard, A.J., Bambrick, J., Bodenstein, S.W., Evans, D.A., Hung, C.-C., O'Neill, M., Reiman, D., Tunyasuvunakool, K., Wu, Z., Žemgulytė, A., Arvaniti, E., Beattie, C., Bertolli, O., Bridgland, A., Cherepanov, A., Congreve, M., Cowen-Rivers, A.I., Cowie, A., Figurnov, M., Fuchs, F.B., Gladman, H., Jain, R., Khan, Y.A., Low, C.M.R., Perlin, K., Potapenko, A., Savy, P., Singh, S., Stecula, A., Thillaisundaram, A., Tong, C., Yakneen, S., Zhong, E.D., Zielinski, M., Bapst, V., Kohli, P., Jaderberg, M., Hassabis, D., Jumper, J.M., 2024. Accurate structure prediction of biomolecular interactions with AlphaFold 3. Nature 630, 493–500. https://doi.org/10.1038/s41586-024-07487-w

Ansari, S., Troelenberg, N., Dao, V.A., Richter, T., Bucher, G., Klingler, M., 2018. Double abdomen in a short-germ insect: Zygotic control of axis formation revealed in the beetle,Tribolium castaneum. Proc. Natl. Acad. Sci. 115, 1819–1824. https://doi.org/10.1073/pnas.1716512115

Barnett, A.A., Nakamura, T., Extavour, C.G., 2019. Hox genes limit germ cell formation in the short germ insect,Gryllus bimaculatus. Proc. Natl. Acad. Sci. 116, 16430–16435. https://doi.org/10.1073/pnas.1816024116

Bregman, D.B., Du, L., Zee, S. van der, Warren, S.L., 1995. Transcription-dependent redistribution of the large subunit of RNA polymerase II to discrete nuclear domains. J. cell Biol. 129, 287–298. https://doi.org/10.1083/jcb.129.2.287

Butt, F.H., 1949. Embryology of the Milkweed Bug, Oncopeltus fasciatus (Hemiptera). Cornell Experiment Station Memoir 3–43.

Colonnetta, M.M., Lym, L.R., Wilkins, L., Kappes, G., Castro, E.A., Ryder, P.V., Schedl, P., Lerit, D.A., Deshpande, G., 2021. Antagonism between,germ cell-less,and Torso receptor regulates transcriptional quiescence underlying germline/soma distinction. eLife 10, e54346. https://doi.org/10.7554/elife.54346

Donoughe, S., Kim, C., Extavour, C.G., 2018. High-throughput live-imaging of embryos in microwell arrays using a modular specimen mounting system. Biol. Open 7, bio031260. https://doi.org/10.1242/bio.031260

Donoughe, S., Nakamura, T., Ewen-Campen, B., Green, D.A., Henderson, L., Extavour, C.G., 2014. BMP signaling is required for the generation of primordial germ cells in an insect. Proc. Natl. Acad. Sci. 111, 4133–4138. https://doi.org/10.1073/pnas.1400525111

Duncan, E.J., Benton, M.A., Dearden, P.K., 2013. Canonical terminal patterning is an evolutionary novelty. Dev. Biol. 377, 245–261. https://doi.org/10.1016/j.ydbio.2013.02.010

Edgar, R.C., 2004. MUSCLE: multiple sequence alignment with high accuracy and high throughput. Nucleic Acids Res. 32, 1792–1797. https://doi.org/10.1093/nar/gkh340

Ewen-Campen, B., Donoughe, S., Clarke, D.N., Extavour, C.G., 2013a. Germ cell specification requires zygotic mechanisms rather than germ plasm in a basally branching insect. Curr. Biol. 23, 835–842. https://doi.org/10.1016/j.cub.2013.03.063

Ewen-Campen, B., Jones, T.E.M., Extavour, C.G., 2013b. Evidence against a germ plasm in the milkweed bug,Oncopeltus fasciatus, a hemimetabolous insect. Biol. Open 2, 556–568. https://doi.org/10.1242/bio.20134390

Ewen-Campen, B., Schwager, E.E., Extavour, C.G., 2010. The molecular machinery of germ line specification. Mol. Reprod. Dev. 77, 3–18. https://doi.org/10.1002/mrd.21091

Extavour, C.G., Akam, M., 2003. Mechanisms of germ cell specification across the metazoans: epigenesis and preformation. Development 130, 5869–5884. https://doi.org/10.1242/dev.00804

Gupta, T., Extavour, C.G., 2013. Identification of a putative germ plasm in the amphipod,Parhyale hawaiensis. EvoDevo 4, 34. https://doi.org/10.1186/2041-9139-4-34

Huettner, A.F., 1923. The origin of the germ cells in,Drosophila melanogaster. J. Morphol. 37, 385–423. https://doi.org/10.1002/jmor.1050370204

Illmensee, K., Mahowald, A.P., 1974. Transplantation of posterior polar plasm in,Drosophila. Induction of germ cells at the anterior pole of the egg. Proc. Natl. Acad. Sci. 71, 1016–1020. https://doi.org/10.1073/pnas.71.4.1016

Jones, D.T., Taylor, W.R., Thornton, J.M., 1992. The rapid generation of mutation data matrices from protein sequences. Bioinformatics 8, 275–282. https://doi.org/10.1093/bioinformatics/8.3.275

Jongens, T.A., Ackerman, L.D., Swedlow, J.R., Jan, L.Y., Jan, Y.N., 1994. Germ cell-less encodes a cell type-specific nuclear pore-associated protein and functions early in the germ-cell specification pathway of Drosophila. Genes Dev. 8, 2123–2136. https://doi.org/10.1101/gad.8.18.2123

Jongens, T.A., Hay, B., Jan, L.Y., Jan, Y.N., 1992. The germ cell-less,gene product: A posteriorly localized component necessary for germ cell development in,Drosophila. Cell 70, 569–584. https://doi.org/10.1016/0092-8674(92)90427-e

Kimura, T., Ito, C., Watanabe, S., Takahashi, T., Ikawa, M., Yomogida, K., Fujita, Y., Ikeuchi, M., Asada, N., Matsumiya, K., Okuyama, A., Okabe, M., Toshimori, K., Nakano, T., 2003. Mouse Germ cell-less as an essential component for nuclear integrity. Mol. Cell. Biol. 23, 1304–1315. https://doi.org/10.1128/mcb.23.4.1304-1315.2003

Leatherman, J.L., Kaestner, K.H., Jongens, T.A., 2000. Identification of a mouse,germ cell-less,homologue with conserved activity in,Drosophila. Mech. Dev. 92, 145–153. https://doi.org/10.1016/s0925-4773(99)00335-4

Leatherman, J.L., Levin, L., Boero, J., Jongens, T.A., 2002. germ cell-less,acts to repress transcription during the establishment of the Drosophila germ cell lineage. Curr. Biol. 12, 1681–1685. https://doi.org/10.1016/s0960-9822(02)01182-x

Moore, J., Han, H., Lasko, P., 2009. Bruno negatively regulates,germ cell-less,expression in a BRE-independent manner. Mech. Dev. 126, 503–516. https://doi.org/10.1016/j.mod.2009.04.002

Nakamura, T., Extavour, C.G., 2016. The transcriptional repressor Blimp-1 acts downstream of BMP signaling to generate primordial germ cells in the cricket,Gryllus bimaculatus. Development 143, 255–263. https://doi.org/10.1242/dev.127563

Pae, J., Cinalli, R.M., Marzio, A., Pagano, M., Lehmann, R., 2017. GCL and CUL3 Control the Switch between Cell Lineages by Mediating Localized Degradation of an RTK. Dev. Cell 42, 130-142.e7. https://doi.org/10.1016/j.devcel.2017.06.022

Panfilio, K.A., Jentzsch, I.M.V., Benoit, J.B., Erezyilmaz, D., Suzuki, Y., Colella, S., Robertson, H.M., Poelchau, M.F., Waterhouse, R.M., Ioannidis, P., Weirauch, M.T., Hughes, D.S.T., Murali, S.C., Werren, J.H., Jacobs, C.G.C., Duncan, E.J., Armisén, D., Vreede, B.M.I., Baa-Puyoulet, P., Berger, C.S., Chang, C., Chao, H., Chen, M.-J.M., Chen, Y.-T., Childers, C.P., Chipman, A.D., Cridge, A.G., Crumière, A.J.J., Dearden, P.K., Didion, E.M., Dinh, H., Doddapaneni, H.V., Dolan, A., Dugan, S., Extavour, C.G., Febvay, G., Friedrich, M., Ginzburg, N., Han, Y., Heger, P., Holmes, C.J., Horn, T., Hsiao, Y., Jennings, E.C., Johnston, J.S., Jones, T.E., Jones, J.W., Khila, A., Koelzer, S., Kovacova, V., Leask, M., Lee, S.L., Lee, C.-Y., Lovegrove, M.R., Lu, H., Lu, Y., Moore, P.J., Munoz-Torres, M.C., Muzny, D.M., Palli, S.R., Parisot, N., Pick, L., Porter, M.L., Qu, J., Refki, P.N., Richter, R., Rivera-Pomar, R., Rosendale, A.J., Roth, S., Sachs, L., Santos, M.E., Seibert, J., Sghaier, E., Shukla, J.N., Stancliffe, R.J., Tidswell, O., Traverso, L., Zee, M. van der, Viala, S., Worley, K.C., Zdobnov, E.M., Gibbs, R.A., Richards, S., 2019. Molecular evolutionary trends and feeding ecology diversification in the Hemiptera, anchored by the milkweed bug genome. Genome Biol. 20, 64. https://doi.org/10.1186/s13059-019-1660-0

Robertson, S.E., Dockendorff, T.C., Leatherman, J.L., Faulkner, D.L., Jongens, T.A., 1999. germ cell-less,is required only during the establishment of the germ cell lineage of,Drosophila,and has activities which are dependent and independent of its localization to the nuclar envelope. Dev. Biol. 215, 288–297. https://doi.org/10.1006/dbio.1999.9453

Schoppmeier, M., Schröder, R., 2005. Maternal Torso Signaling Controls Body Axis Elongation in a Short Germ Insect. Curr. Biol. 15, 2131–2136. https://doi.org/10.1016/j.cub.2005.10.036

Skelly, J., Pushparajan, C., Duncan, E.J., Dearden, P.K., 2019. Evolution of the Torso activation cassette, a pathway required for terminal patterning and moulting. Insect Mol. Biol. 28, 392–408. https://doi.org/10.1111/imb.12560

Tamura, K., Stecher, G., Kumar, S., 2021. MEGA11: Molecular Evolutionary Genetics Analysis Version 11. Mol. Biol. Evol. 38, 3022–3027. https://doi.org/10.1093/molbev/msab120

Warren, S.L., Landolfi, A.S., Curtis, C., Morrow, J.S., 1992. Cytostellin: a novel, highly conserved protein that undergoes continuous redistribution during the cell cycle. J. Cell Sci. 103, 381–388. https://doi.org/10.1242/jcs.103.2.381

Weisbrod, A., Cohen, M., Chipman, A.D., 2013. Evolution of the insect terminal patterning system—Insights from the milkweed bug,Oncopeltus fasciatus. Dev. Biol. 380, 125–131. https://doi.org/10.1016/j.ydbio.2013.04.030

Ylla, G., Nakamura, T., Itoh, T., Kajitani, R., Toyoda, A., Tomonari, S., Bando, T., Ishimaru, Y., Watanabe, T., Fuketa, M., Matsuoka, Y., Barnett, A.A., Noji, S., Mito, T., Extavour, C.G., 2021. Insights into the genomic evolution of insects from cricket genomes. Commun. Biol. 4, 733. https://doi.org/10.1038/s42003-021-02197-9